Investigation of sizing - from glass fibre surface to composite interface

Petersen, Helga Nørgaard; Almdal, Kristoffer; Brøndsted, Povl; Kusano, Yukihiro; Sørensen, Bent F.

Publication date:
2017

Document Version
Publisher's PDF, also known as Version of record

Investigation of sizing - from glass fibre surface to composite interface

Helga Nørgaard Petersen
PhD Thesis February 2017

DTU Nanotech
Department of Micro- and Nanotechnology

Investigation of sizing - from glass fibre surface to composite interface

PhD thesis

HELGA NØRGAARD PETERSEN
Department of Micro- and Nanotechnology
Technical University of Denmark

FEBRUARY 2017
DTU NANOTECH & DTU WIND ENERGY

Prepared by:
Helga Nørgaard Petersen

Main supervisors:
Kristoffer Almdal, Professor
Technical University of Denmark
DTU Nanotech
Mail: kral@nanotech.dtu.dk

Povl Brøndsted, Professor
Technical University of Denmark
DTU Wind Energy, Section of Composites and Material Mechanics
Mail: pobr@dtu.dk

Yukihiro Kusano, Senior Scientist
Technical University of Denmark
DTU Wind Energy, Section of Composites and Material Mechanics
Mail: yuki@dtu.dk

Technical University of Denmark
DTU Nanotech
Ørstedsplads 345E
2800 Kgs. Lyngby
Denmark
Tel +45 4525 5700
Mail: info@nanotech.dtu.dk
Web: http://www.nanotech.dtu.dk/

Publication reference data
Helga Nørgaard Petersen
Investigation of sizing – from glass fibre surface to composite interface
PhD thesis
Technical University of Denmark
DTU Nanotech
February 2017

Preface

This thesis is submitted in candidacy for the Ph.D.-degree from Technical University of Denmark.

The presented work was carried out from January 2013 to February 2017 as a collaboration between the research group Amphiphilic Polymers in Biological Sensing under the Department of Micro- and Nanotechnology (DTU Nanotech, Lyngby) and the section of Composites and Material Mechanics under the Department of Wind Energy (DTU Wind Energy, Roskilde).

The project was a part of the Danish Centre for Composite Structures and Materials for Wind Turbines (DCCSM) financed by the Danish Research Council for Strategic Research (grant number: 09-067212).

The project was supervised by Professor Kristoffer Almdal (DTU Nanotech) and co-supervised by Professor Povl Brøndsted (DTU Wind Energy) and Yukihiro Kusano (DTU Wind Energy).

As a part of the ph.d.-study a research stay was completed at University of Strathclyde (Glasgow, United Kingdom) from April to September 2014 in the Advanced Composites Group lead by Professor James L. Thomason. The research stay was made possible through financial support by Oticon Fonden, Otto Mønsteds fond, Augustinus Fond and Knud Højgaards Fond.

Helga Nørgaard Petersen

Risø, Denmark
February 2017

Acknowledgements

First of I would like to thank all my many supervisors, official and unofficial (Kristoffer, Povl, Yuki and Bent), for giving me this opportunity, for support and guidance throughout the project and for letting me stand on my own feet. A special thanks to Yuki for proofreading every little thing and swiftly.

Another special thanks goes to Prof. Thomason for letting me visit his research group and to all the group members for the warm welcome. Also thanks to Ross Minty a fellow sufferer when it comes to the almost impossible work with nearly invisible single glass fibres and likewise microdroplets, it is always easier when you have company.

A large thanks to my group members in PolSens and colleagues at DTU Nanotech for invaluable help in the lab, good discussions and lunches. Thank you, Sergey, Andriy, Sanjukta, Anders, Saif, Sanaullah, Alexandra, Lars, Lotte, Ole, Tine, Matilda and many more.

My colleagues at Risø (COM) deserves the greatest of gratitude for making me feel at home. Thanks to Hønsegården, Justine, Kristine and Lucie, for all the talking, beer and discussions technical and other indifferences. Thanks to Fiberlab/the minions, Jonas, Christian and Jacob, I owe you everything in this thesis. It would not have been the same without you. A big thanks for putting up with my curiosity and blabbering mouth. In general just a huge appreciation of all the open doors I have come bursting through with questions, that you gladly answered.

I would also like to thank Rød stue, the rest of the gang and a few ninjas for letting me know that there are other things in life than work, especially in the last part of my Ph.D.-study.

I am grateful for my family and all the help and support they have given me. Thanks for always believing in me no matter what.

My last but far from smallest thanks goes to my one and only Rasmus and our son Arthur, for always being there and for giving me your endless love.

Abstract

Composites are far from a new invention, and have through time taken many shapes. From a simple hay clay house to advanced nano particle containing composites for advanced material applications. Since the industrialisation in the late 1800's the use of fibre reinforced composites have increased significantly. The usage span wide, from furniture and car components to construction materials. Even though, the concept of composites is well known and widely applied, the fundamental principles of the interaction of the constituents, in the composites are still not fully understood. This thesis is a part of Danish Center for Composite Structures and Materials for wind turbine blades who work towards improving composites. Since wind turbine blades are the basis of the DCCSM it is the materials used here that are the focus, explicitly glass fibres and epoxy matrix. Glass fibre composites greatly dominate the fibre reinforced composite industry due to the combination of their relatively high stiffness and low production cost. During manufacturing the glass fibres are applied a coating, called sizing, for protection of the fibres and for compatibility with the polymer matrix. The sizing is located at the interface between glass fibre and polymer matrix. Despite the importance of this interface, in regards to the stress transfer, which is responsible for the reinforcing effect of fibres, very little research address how the interface is affected and how it can be controlled. This thesis covers an analysis of the sizing from the glass fibre surface to the interface in composites.

Through soxhlet extraction with acetone it was possible to remove a part of the sizing from the glass fibres for analysis. By burning off the sizing at 565 °C a higher mass loss was obtained than from the extraction, indicating that a part of the sizing might be covalently bonded to the glass fibre surface. The investigation of the sizing extract by ATR-FTIR and TGA-MS revealed the presence of a DGEBA film former as one of the components of the sizing. Glass plates were successfully coated with the organosilanes APTMS and GPTMS in order to mimic the surface of the glass fibres. The non-planar surface of glass fibres yields difficulties in some analysis e.g. determination of contact angle. The plates displayed a clear difference in contact angle after being coated towards a more polar surface.

An investigation of the adhesion between fibre and matrix analysed by microbond testing and the determination of the IFSS was conducted varying the amine:epoxide group ratio in the matrix and the testing temperature. IFSS was found to be affected by both parameters. A maximum IFSS was observed around the stoichiometric ratio of amine:epoxide group (1:1). The presence of amine or epoxide groups in the sizing will affect the ratio at the interface and in all probability also the IFSS with a decrease in IFSS as the result. Furthermore, the testing temperature influenced the IFSS. The highest values were obtained at room temperature. Above the glass transition temperature the dependency of the amine:epoxide group ratio changed to become linear. Two different microbond setups were used for the determination of the IFSS and a difference was detected. It was explained by the difference in loading procedure; one had constant strain rate and the other constant load rate. Additionally the duration of the microbond test might also influence the determination of the IFSS.

The influence on the mechanical properties stiffness, strength and J-integral by changes in the chemistry of the interface was investigated. The stiffness of single glass fibres increased after the removal of sizing by extraction but also when the sizing was removed by burning. This could partly be explained by the sizing being less dense than the glass fibres. For the

burned glass fibres compactment of the glass structure also yields an increase in stiffness. The fibre strength was less affected by the extraction of sizing but burning drastically decreased the strength. The enlargement of surface flaws after the removal of the protective sizing is given as the cause of the decrease in strength. Coating of fibres after extraction of the original sizing by the organosilane GPTMS resulted only in insignificant changes of stiffness and strength of single glass fibres. However the effect on the adhesion measured by the J-integral was remarkable. Small scale specimens were successfully used for the DCB testing and the determination of the J-integral. The GPTMS modified fibres displayed significant higher interface adhesion in comparison to the fibres with the original sizing. From this it had been proved that the original sizing is far from the optimal when it comes to facilitating a strong adhesion between glass fibre and matrix.

Resumé

Kompositter er langt fra en ny opfindelse og har gennem tiden haft mange former. Fra simple hør-ler hytter til avancerede nanopartikel kompositter. Siden industrialiseringen sent i 1800-tallet er brugen af kompositter steget markant. Brugen af kompositter spænder vidt fra møbler og bildele til bygningsmaterialer. På trods af at komposit konceptet er velkendt og vidt anvendt, er de fundamentale principper for interaktionen mellem bestanddelene i kompositter stadig ikke fuldt ud forstået. Denne afhandling er en del af Danish Center for Composite Structures and Materials for wind turbine blades der arbejder mod at forbedre kompositter. Eftersom vindmøllevinger er grunddelen af DCCSM er det de materialer der bruges her som fokuseres på. Helt specifikt er det glasfibre og epoxy matrice. Glasfiber kompositter dominerer i høj grad industrien for fiberforstærkede kompositter grundet kombinationen af deres relative høje stivhed og lave produktionsomkostninger. Under fremstillingen af glasfibre bliver de overfladebehandlet med en coating, kaldet sizing, for at beskytte glasfibrene og for at sikre kompatibilitet med polymer matricen. Sizingen befinder sig i grænsefladen mellem glasfiber og polymer matrice. Denne grænseflade er vigtig i forhold til belastningsoverførsel mellem fiber og matrice, hvilket er baggrunden for den forstærkende effekt af fibrene i kompositter. På trods af dette findes der kun ganske lidt litteratur omhandlende hvordan grænsefladen påvirkes og hvordan den kan kontrolleres. Denne afhandling dækker analyse af sizingen fra glasfiberoverfladen til grænsefladen i kompositter.

Gennem soxhlet ekstraktion med acetone var det muligt at fjerne en del af sizingen fra glasfibre til efterfølgende analyse. Afbrænding ved 565 °C blev et større vægttab opnået end ved ekstraktion, dette indikerer at en del af sizingen kunne være kovalent bundet til glasfiberoverfladen. Undersøgelsen af sizing ekstraktet ved ATR-FTIR og TGA-MS afslørede tilstedeværelsen af en DGEBA film former som en af sizing komponenterne. Glasplader blev succesfuldt overfladebehandlet med organosilanerne APTMS og GPTMS for at efterligne glasfiberoverfladen. Den ikke plane glasfiberoverflade giver anledning til vanskeligheder i forhold til nogle analyser som fx bestemmelsen af kontaktvinklen. Pladerne udviste en klar ændring i kontaktvinkel efter overfladebehandlingen mod en mere polær overflade.

Undersøgelsen af vedhæftningen mellem fiber og matrice analyseret ved microbond testning og bestemmelsen af IFSS blev udført med varierende amin:epoxy gruppe ratio i matricen og med varierende testtemperatur. Det blev fundet at IFSS blev påvirket af begge parametre. En maksimal IFSS blev fundet ved den støkiometriske ratio af amin:epoxy gruppe (1:1). Tilstedeværelsen af amin eller epoxy grupper i sizingen vil påvirke ration i grænsefladen hvilket med stor sandsynlighed også IFSS med en aftagning i IFSS som resultat. Ydermere påvirker testtemperaturen også IFSS. De højeste værdier blev opnået ved stuetemperatur. Over glas transitions temperatur ændrede afhængigheden af amin:epoxy gruppe ratioen sig til at blive lineær. To forskellige opsætninger blev brugt til bestemmelsen af IFSS of en markant forskel blev detekteret. Denne blev forklaret med forskellen i last proceduren, en med konstant tøjningsrate og en med konstant lastrate. Oveni er det muligt at varigheden af microbond testen også påvirker bestemmelsen af IFSS.

Indflydelsen af ændringer i den kemiske sammensætning i grænsefladen på stivhed, styrke og J-integralet blev undersøgt. Stivheden af enkelte glasfibre steg efter fjernelse af sizing ved ekstraktion men også når sizingen blev fjernet ved afbrænding. Dette kunne til dels forklares med at sizingen har lavere densitet end glasfibrene. For de brændte fibre giver fortætningen

af glasstrukturen også en stigning i stivhed. Fibre styrken blev i mindre grad påvirket af ekstraktionen af sizingen, mens afbrænding drastisk reducerede styrken. Forstørrelsen af overfladedefekter efter fjernelse af den beskyttende sizing er angivet som årsagen til faldet i styrke. Overfladebehandlingen af fibre med organosilanen GPTMS efter ekstraktionen af den originale sizing resulterede ikke i signifikante ændringer i hverken stivhed eller styrke af enkelte glasfibre. Der var dog en tydelig effekt på vedhæftningen målt ved J-integralet. Mini emnerne blev med stor succes anvendt til DCB tests og bestemmelsen af J-integralet. Fibrene modificeret med GPTMS udviste signifikant højere grænseflade vedhæftning i forhold til fibre med den originale sizing. Af dette blev det bevist at den originale sizing er langt fra optimal når det kommer til at fremme en stærk vedhæftning mellem glasfibre og matrice.

List of Publications

This thesis is based on the following papers, which are referred to in the text by Roman numerals.

Paper I: Petersen, H.N., Kusano, Y., Brøndsted, P., Almdal, K., Investigation of physisorbed and covalent bonded sizing on commercial E-glass fibres. *Submitted* (2017)

All of the experimental work, analysis, and main part of writing. First author of the paper.

Paper II: Petersen, H.N., Minty, R.F., Thomason, J.L., The amine:epoxide ratio at the interface of a glass fibre/epoxy matrix system and its influence on the interfacial shear strength *Submitted* (2017)

Conducted the experimental work and analysis together with Ph.D.-fellow Ross Minty, main part of writing. First author of the paper.

Paper III: Minty, R.F., Petersen, H.N., Thomason, J.L., The role of matrix stoichiometry on the interfacial strength in glass fibre reinforced epoxy composites *Submitted* (2017)

Contributed to this paper with planning and co-working on the initial experimental work and part of writing. Second author of the paper.

Paper IV: Petersen, H.N., Kusano, Y., Brøndsted, P., Almdal, K., The influence of removing sizing on strength and stiffness of conventional and high modulus E-glass fibres. *IOP Conf. Series: Materials Science and Engineering* **139**, 012040 (2016)

All of the experimental work, analysis, and main part of writing. First author of the paper.

Nomenclature

Abbreviation		
APTMS	(3-Aminopropyl)trimethoxysilane	
ATR	Attenuated Total Reflectance	
CA	Contact Angle	[°]
DCB	Double Cantilever Beam	
DGEBA	Bisphenol A diglycidyl ether	
DSC	Differential Scanning Calorimetry	
EXT	Laminate and DCB speimens manufactured from fabrics where the sizing is extracted	
FTIR	Fourier Transform Infrared spectroscopy	
GPTMS	(3-Glycidyloxypropyl)trimethoxysilane	
IFSS	Interfacial Shear Stress	[GPa]
LVDT	Linear variable differential transformer	
MOD	Laminate and DCB speimens manufactured from fabrics where GPTMS is applied as sizing	
MS	Mass Spectroscopy	
REF	Laminate and DCB speimens manufactured from fabrics with the original sizing	
TETA	Triethylenetetramine	
TGA	Thermogravimetric Analysis	
TMA	Thermomechanical Analysis	
UD	Unidirectional	

Greek symbols		
γ^{d}	Dispersive components of the surface energy	[mJ·m^{-2}]
γ^{p}	Polar components of the surface energy	[mJ·m^{-2}]
δ	Displacement	[mm]
δ^*	Displacement at the crack tip	[mm]
ΔL	Elongation/extension	[μm]
θ	Contact angle	[°]
μ	Linear density	[g/m]
ν	Poisson's ratio	[-]
$\rho_{composite}$	Density of composite	[g/cm^3]
ρ_{fibre}	Density of fibre	[g/cm^3]
ρ_{matrix}	Density of matrix	[g/cm^3]
$\rho_{sealing}$	Density of sealing	[g/cm^3]
ρ_{water}	Density of water	[g/cm^3]
σ_b	Bridging stress	[Pa]
τ_s	Shear stress	[Pa]

Roman symbols

A	Cross sectional area	[μm^2]
A_e	Embedded area	[1000 μm^2]
B	Height of DCB sample	[mm]
d	Moment arm	[mm]
d_f	Diameter of fibre	[μm]
E_{11}	Longitudinal stiffness of composite	[GPa]
E_{fibre}	Stiffness of fibre	[GPa]
E_{matrix}	Stiffness of matrix	[GPa]
f	Frequency	[s^{-1}]
F	Load	[N]
F	Tension (for tensile test)	[N]
F_{max}	Maximum load	[N]
H	Beam width of DCB specimen	[mm]
J	J-integral, non-linear energy release rate	[J/m^2]
L_e	Droplet length / embedded fibre length	[μm]
L_g	Gauge length	[mm]
m_{fibre}	Mass of fibre	[g]
$m_{sample,a}$	Mass of volume fraction sample in air	[g]
$m_{sample,s}$	Mass of volume fraction sample sealed in air	[g]
$m_{sample,w}$	Mass of volume fraction sample sealed in water	[g]
M	Moment	[J]
P	Load	[N]
T	Tension (for linear density)	[N]
Tg	Glass transition temperature	[°C]
V_{fibre}	Volume fraction of fibre	[%]
V_{matrix}	Volume fraction of matrix	[%]
$V_{porosity}$	Volume fraction of porosity	[%]
W_{fibre}	Weight fraction of fibre	[%]
W_{matrix}	Weight fraction of matrix	[%]

Contents

1 Introduction

In this chapter the topic and the motivation of the thesis will be presented along with the aim and scope of the study.

1.1 Motivation

Composites have been used in many ways and for hundreds of years from hay in clay construction material by the ancient Mayan civilisations to nanofillers in polymers for dental fillings of today [1–3]. They are not always labeled as composites but by the definition they are. A composite is made from at least two components with considerably different properties, this being chemically and/or physically [1, 4]. With the industrialisation in the late 1800's came synthetic polymers as melamine and Bakelite. Additionally the first commercially processed glass fibres introduced by Owens Corning in the late 1930's. The building blocks for fibre reinforced polymer composites were laid. It quickly developed from there and today composites are widely used from the automotive industry to the wind energy industry. The main reason for the popularity is the unique mechanical behaviour that these materials possess: elasticity from the matrix and strength from the reinforcement yielding high strength and stiffness combined with low density [1, 5, 6]. Glass fibre reinforced polymers is a type of composites that are highly used [7]. The low price of glass fibres makes them outpace carbon fibres, despite their superior stiffness [5]. In all composite using industries the demands for better mechanical properties give rise to a large interest in how to improve and optimise stiffness and strength especially in regard to fatigue and impact. The research focus to great extent on structure design, orientation of fibre layup, optimising manufacturing parameters, and testing properties of new constituent materials [8]. Compared to this, very little research address how the interface between matrix and reinforcement can be controlled and used for improving the overall mechanical properties of the composite [7]. At the interface a diffuse element exist: sizing, which might be why researchers are reluctant to grapple with investigating it. Furthermore a challenge is that it seems as the topic falls between the two scientific fields of chemistry and mechanical engineering, who look at composites in two very different ways. Chemists look at what compounds are present at the interface and possible reactions where mechanical engineers consider the interface merely the region where the stress transfer between matrix and reinforcement occurs. The essence of this challenge is that mechanical engineers and chemists rarely share the knowledge they each possess on the topic. Combining the knowledge could result in a leap towards improving the composites straight from the interface.

The diffuse element at the interface is called sizing, which is both the name of the aqueous suspension and the process of applying it. The exact composition of sizing is kept a trade secret, where patents provide a very narrow window into it, but most often it is almost impossible to understand and study [7, 9, 10]. The secrecy surrounding the sizing adds to obstacles on the path towards more knowledge about the interface leading to improvement of the composite. Glass fibre manufacturers label their products in regard to which matrices they are suitable for and compatible with, but does not include other parameters about the sizing that could affect the final properties of the composite. However, the manufactures of glass fibres do not always know what the sizing consists of, and in even less extent the manufactures of matrices and certainly the composite producers do not know. In general the composite manufacture is based on practical experience, when it comes to sizing, and if it works there is little interest in why or if it could be improved. Of course sizing is being optimised and investigated but primarily the industry within itself. Both Owens Corning and Michelman advertise fibres with increased adhesion to the matrix with an increased composite strength as the result [11, 12].

1.2 Aim and scope

This project is a collaboration between DTU Nanotech and DTU Wind energy supported by Danish Centre for Composite Structures and Materials for wind turbines (DCCSM), which works towards methods for improving composites for wind turbine blades. This project is part of the work package related to Nano-/microscale with the interface as focus. The project is more than a departmental collaboration as it combines the scientific fields of chemistry and mechanical engineering; going from mechanics of large composite wind turbine blades to the nanoscale of chemistry as illustrated in fig. 1.1. This link to the wind energy industry means that the material and manufacturing focus in this thesis is on those mainly used there e.g. continuous glass fibres and epoxy resin matrices by vacuum infusion.

The aim is to obtain more knowledge on sizing and how to control the interface and hereby the large scale material properties. The sizing is the key to control as is clearly illustrated in fig. 1.2. In general for structual applications a strong interface is preferable [15]. One issue is to control the interface by optimizing the sizing, another issue is how to quantify this improvement. The difference between a strong and a weak interface is visualised in fig. 1.2, but a numerical value like the interfacial shear strength (IFSS) would be preferable since the phenomenon can be qualitatively assessed. Methods that only require a minimum of material, but still deliver results, that can differentiate between various treatments of the fibres would have an advantage. As manufacturing and testing a large number of individual modified samples is costly. The droplet microbond, single fibre pull-out and single fibre fragmentation test are such tests where only single fibres are used. The values obtained from micro scale of IFSS might not be directly comparable with e.g. interlaminar shear strength, but these micro samples will although be a guideline when going from small scale to large scale.

1.3 Overview of the thesis

Chapter 2 presents the background on the materials used and the theory of the interface. Chapter 3 lists the materials and equipment used, the methods and settings are mentioned in connection to the individual investigations. Chapter 4 presents the characterisation and

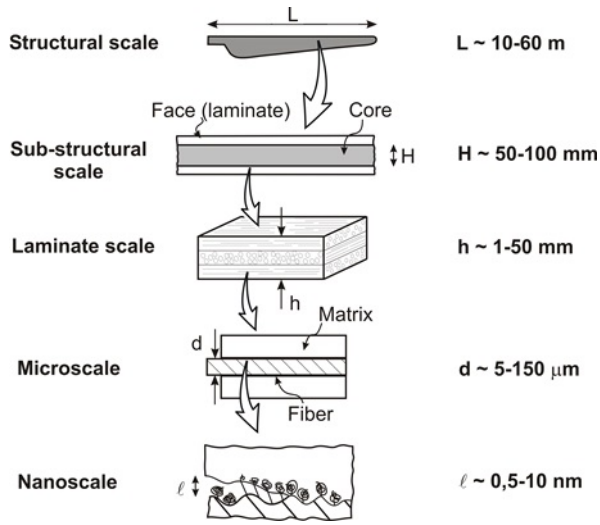

Figure 1.1: Illustrading the different length scales of a composite for wind turbine blades covered by the DCCSM project from structural components to the interface between fibre and matrix. Adapted from [13] by Bent F. Sørensen.

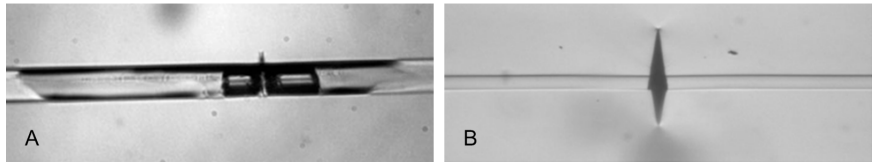

Figure 1.2: Same type of fibre in two different matrices. The fibre with a sizing compatible with an epoxy matrix in A) a polyester matrix and B) an epoxy matrix. A) A weak interface: debonding at the fibre/matrix interface. B) Strong interface: crack propagates into the matrix. Source: Stefanie Feih, during the work with Single Fibre Fragmentation Test [14].

analysis of sizing on glass surfaces. Chapter 5 presents the investigation of the sizing in the interface. Chapter 6 presents the effect of sizing investigated. The concluding remarks and future work/outlook are in chapter 7, followed by the used references listed sequentially and an appendix containing the papers written as a part of the project.

2 Background

In this thesis sizing is investigated through three scenarios: as a surface coating, as a link between fibre and matrix, and finally as the adhesion between composite constituents. This chapter presents; background knowledge on the used composite constituents, sizing and the interface.

2.1 Glass fibre reinforced polymers

Composites are used in many industries from car components, furnitures, construction materials to boats and wind turbine blades. The materials used for composites can be selected in accordance with manufacturing process, desired properties, and price. A composite for structural application is a filler added to a bulk material to improve the properties of the bulk by reinforcement. Glass fibres are neither the strongest nor the stiffest but the price is low compared to e.g. carbon fibres that are superior in stiffness. Despite that glass fibres have been used in composites for more than 80 years they are still by far the most used reinforcement and currently less than 5 % of fibres used by the composite industry is something other than glass fibres [7]. These include aramid, polylactic acid (PLA), and natural fibres as hemp and jute which are mostly used for smaller components [16]. A new trend in composites is to manufacture hybrid composites using e.g. both glass and carbon fibres. The glass fibres are then used for the main part and the carbon fibres for the parts that need high stiffness e.g. the highly strained outer parts of a wind turbine blade.

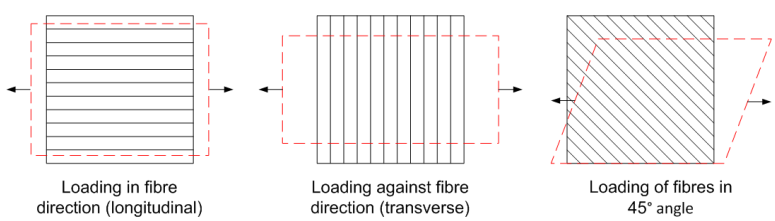

Figure 2.1: The deformation depending on the fibre orientation: longitudinal, transverse and 45° angled.

A large part of composites are used for construction materials. Where construction materials as steel and aluminium in general are homogeneous materials; composite materials on the other hand are not the same in all directions, thus inhomogeneous materials. Applying tension can lead to shear deformation to a lesser or greater extent depending on the direction

of the reinforcement, see fig. 2.1. Composites using continuous fibres have superior mechanical properties in the direction parallel with the fibres (longitudinal direction) compared to the directions perpendicular to the fibres (transverse direction) where the matrix is the decisive component. Continuous glass fibres in the form of woven fabrics are a very common way of introducing the reinforcement in the composite, which is referred to as a laminate. The fabrics can be unidirectional (UD), biaxial or random, often a combination is used or woven in special patterns to increase the strength in certain directions. UD laminates with a lay-up where all the fibres are oriented in one direction are very stiff and strong but only in the longitudinal direction. A composite with a lay-up of stacked fabric where the fibres are oriented in various angles results in a laminate with improved properties in the transverse directions. Increasing the amount of glass fibres in a composite, also known as the fibre volume fraction, is also directly related to the strength and stiffness of the composite which will increase until a certain point where there is too little matrix to keep the composite together. Usually fibre volume fractions above 70 wt.% is avoided depending on the matrix. The constituents, their orientation and the amounts of them dictate the properties of the final composite, but the manufacturing process also affect the outcome in regards to e.g. curing and void content.

Composites can be manufactured in many different ways depending on the reinforcement and the polymer used from pultrusion to injection moulding. Often vacuum is used as a way of distributing the resin in a fibre lay-up, which can be placed in a mould or on a tool plate acting as a flat mould covered by a vacuum bag [1, 4].

2.2 Polymer matrices

The polymers used for composites are usually either thermosetting or thermoplastic polymers. The difference lies in whether the polymer chains are crosslinked. The chemical crosslinking, that occurs during the curing of thermosetting polymers, ensures a rigid structure that makes it impossible to dissolve or melt for further processing. Thermoplastics on the other hand will melt when exposed to certain solvents and possess the characteristic that they can be moulded under heating [4, 17]. The matrices used for glass fibre reinforced polymers are both thermoplastics and thermossettings. For wind turbine blades mainly thermosettings like polyesters, vinylesters and epoxy polymers are used, this is due to their high failure stain. Epoxy resin is a two component polymer, consisting of a linear epoxy resin polymer and a polyamine curing agent like DGEBA and TETA in fig. 2.2, n refers to the number of repetitive units usually in the range of 2-25 [17].

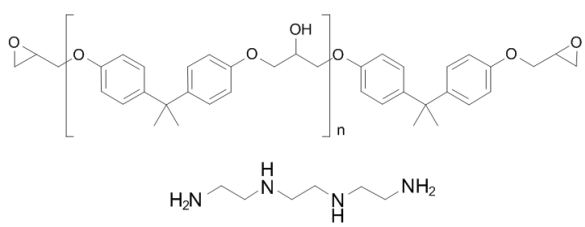

Figure 2.2: The chemical structures of poly(bisphenol-A diglycidylether epoxy resin (DGEBA polymer) and triethylenetetramine (TETA), n is the number of repetitive units. Both are used in this thesis.

When the matrix is curing, the amine and epoxide groups react one to one creating the rigid structure. The epoxy polymer is a long molecule compared to the curing agent. However in regards to the functional groups it is the other way around as the epoxy resin usually contains two epoxide groups, one in each end, where the curing agent contains multiple like the sixfold-functional amine groups in TETA, two primary amines at the ends and two seconday amines in the middle. When primary amines react they become secondary amines. An example of the crosslinked structure of DGEBA and TETA is illustrated in fig. 2.3.

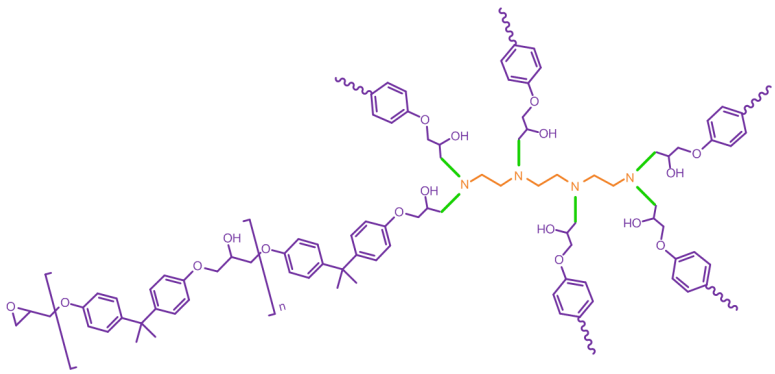

Figure 2.3: The crosslinked structure surrounding the polyamine by reaction of TETA and DGEBA, see section 2.2.

The ratio between the amine and epoxide groups is directly related to the crosslinking density and the physical properties of the final material. To some extent a fully cured epoxy element can be considered one giant molecule. The highest crosslinking density is achieved when all amines and epoxide groups have reacted resulting in a material with high stiffness. The stoichiometric ratio is where the amine and epoxide group ratio is 1:1. This is not equal to a weight ratio of 1:1.

2.3 Manufacturing of glass fibres

Almost all glass fibres are based on silica, that has a very high melting temperature around 2000 °C even though it starts softening at 1200 °C. To reduce the melting temperature different additives are included. Taking the additives into account most glass fibres contain around 55-75wt.% SiO_2, see tab. 2.1. Al_2O_3 and B_2O_3 are so called network formers as they become part of the silica tetrahedral network, but compared to silica they will leave oxygen ions negatively charged. This is solved by adding CaO, BaO, Na_2O or K_2O and will be located near charged oxygen ions to achieve an overall neutrality. These oxides are not a part of the network and are therefore named network modifiers. Adding too much of network modifiers will disturb the network. The ions K^+ and Na^+ can move relatively easily in the network and thus increasing the electricalconductivity of the glass [6, 16].

The low conductivity of E-glass is the main reason for the usage in electrical applications for which it was initially invented, but the chemical durability of the fibres made them excellent as fibre reinforcement. E-glass has a melting temperature of just above 1200 °C at which point the fibres can be drawn. A-glass is cheaper to manufacture than E-glass, but with only half the strength. The content of A-glass is close to what is used for ordinary glass, also

Table 2.1: Different types of glass for fibres and their content of oxides in relation to weight (%). Note that constituent should not be mistaken for the raw material. Adapted from [18].

Constituent	E	A	C	S	R	AR	ECR	D
SiO_2	52-56	63-72	64-68	64-66	55-60	55-75	54-62	72-75
Al_2O_3	12-16	0-6	3-5	24-25	23-28	0-5	9-15	0-1
B_2O_3	5-10	0-6	4-6		0-0.35	0-8		21-24
CaO	16-25	6-10	11-15	0-0.2	8-15	1-10	17-25	0-1
MgO	0-5	0-4	2-4	9.5-10	4-7		0-4	
$Na_2O + K_2O$	0-2	14-16	7-10	0-0.2	0-1	11-21	0-2	0-4
Ti_2O	0-1.5	0-0.6				0-12	0-4	
Zr_2O						1-18		
Fe_2O_3	0-0.8	0-0.5	0-0.8	0-0.1	0-0.5	0-5	0-0.8	0-0.3
F_2	0-1	0-0.4			0-0.3	0-5		
BaO			0-1					
ZnO							2-5	
Li_2O						0-1.5		

called soda-lime glass. C-glass on the other hand is useful in acidic environments where E-glass is neither resistant to acid nor alkalis. S- and R-glass have higher strength, but is much more expensive to manufacture compared to E-glass fibres. AR-glass is applicable in e.g. cements as they are alkali resistant. ECR-glass is a chemically resistant E-glass. D-glass is based on E-glass but with a even lower electrical conductivity to be used in high performance electronic devices [6, 16, 18]. The distribution of the additives in the different types of glass fibre is listed in tab. 2.1.

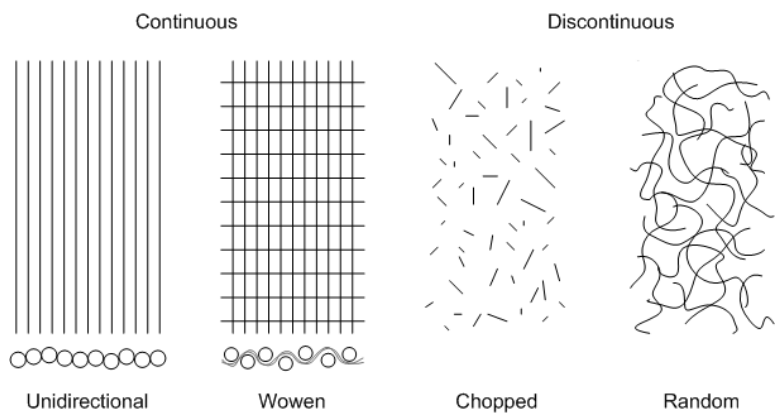

Figure 2.4: Different types of fabric produced from continuous or discontinuous fibres.

For the manufacturing of the fibres all the raw materials are mixed and lead to the furnace where it melts. In a continuous process the melt is then lead directly to the bushing having a large number of holes through which the melt is drawn into fibres. The bushing is made from a platinum–rhodium alloy that decomposes due to the high temperatures. The fibres are drawn continuously throughout the lifetime of the bushing. Immediately after leaving the bushing the glass is rapidly quenched by water being sprayed and drawn to lock the

amorphous structure of the glass, thus avoid the formation of crystallinity. The drawing is carried out with a rate of around 2500 m/min by a rotating drum several meters down from the bushing. The cooling rate is the main responsible for the diameter of the fibres, the draw rate affects the diameter in lesser extend. The drawing process greatly affects properties as density, elastic modulus and chemical resistance [6, 16, 19].

Instantly after being quenched the fibres pass a roller half submersed in the aqueous suspension of sizing, see fig. 2.5. Afterwards the fibres from one or more bushing are collected into a roving which contains 50-4000 single fibres and wound into a roving [6, 16, 19]. The actions taken in the next step depends on the end product, but in general the fibre rovings are either winded or chopped. The continuously winded fibres are then dried in a large oven above 100 °C for hours. The roving is then used for e.g. chopped strand mats, random strand mats or woven mats. The mats are also referred to as fabrics, see fig. 2.4. The woven patterns of fabrics are endless and depend on the desired orientation of the fibres. Most used in the composite industry are the unidirectional (UD), woven and random oriented fabrics [1, 4, 6, 16].

Figure 2.5: Fibres drawn from two bushings passing the sizing applicator roll [20].

2.4 Glass fibre sizing

The sizing is applied to fulfil a number of tasks and demands. The process in which it is applied alone makes limitations to the constituents. They should be able to form a suspension or be dissolved in water in order to be transferred by the applicator roll,as illustrated in fig. 2.5. Water is used as it wets glass easily and fast yielding a good dispersion of the sizing [19]. The aqueous suspension contains 3-10 wt.% solid [6]. Furthermore the constituent should withstand temperatures of around 100 °C for hours without decomposition. The first job of the sizing becomes crucial within seconds of it being applied: protecting the glass fibre

surface against fibre-fibre damage when winded into a strand in order to continue the processing and handling [19]. But the challenges do not stop here, besides the demands related to the processing and handling of the glass fibres there are also the factors of economics, end-purpose and performance of the final product to include. Getting the sizing right means a huge advantage in the competition with other glass fibre manufacturers which is the main reason why the industry is meticulously concealing their recipes. The ideal sizing protects the fibres during processing, reduce fuzz during handling, disperse well on the fibres yielding a homogeneous product, provide good wetting during composite manufacture with a low void content as a result, facilitate high fibre matrix interaction for successful stress transfer and with low expenses [7, 19]. This requires several components and preferable with multiple purposes to reduce the complexity.

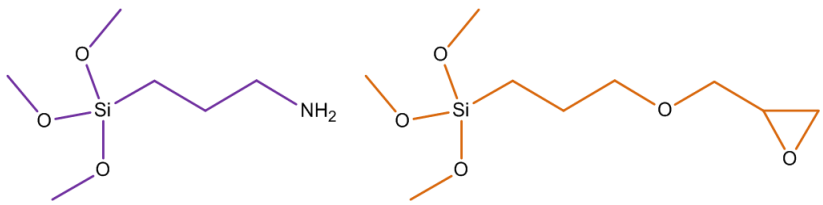

Figure 2.6: Chemical structures of two organosilanes typically used as coupling agents in sizing. (3-aminopropyl)trimethoxysilane (APTMS) and (3-glycidyloxypropyl)trimethoxysilane (GPTMS).

Most sizing consists as a minimum of a film former and a coupling agent, but often many more components. The film former protects against fibre-fibre damage and protects the whole roving during winding and fabric production. It is often chosen to be similar to the matrix, e.g. polyesters, polyurethanes, and epoxies in order to obtain a good wetting. The coupling agent reduce stress corrosion caused by water. Often it is a organosilane but chromium and titanium oxides are also used. Organosilanes have the possibility of reacting with both fibre and matrix and is therefore often chosen. The structures of two organosilanes typically used as coupling agents are displayed in fig. 2.6, both are also used in this thesis. Anti-static agents are added to reduce fuzziness. Emulsifier agents are added to stabilise insoluble components in the suspension and also to counteract foaming and to adapt the viscosity. Lubricants might be added to further improve the dispersion and protect the fibres. Other components might be wetting agents, antioxidants, and acid/base to adjust pH to around 4 to facilitate hydrolysis of silanes [6, 7, 9, 16].

2.5 Interface or interphase

When it comes to the region between the fibre and the matrix it is referred to as either interface or interphase often without any separation between the two expressions. The interface often relates to the actual areas where the fibre and the matrix come into contact whereas the interphase includes the boundaries of the glass and the matrix. A little simplified: interface is two dimensional and interphase is three dimensional. However the presence of sizing blot out the boundaries as it is somewhere between like an interphase in the interphase. In this thesis the expression 'interface' has been chosen to label the zone of fibre and matrix which includes the sizing, see fig. 2.7.

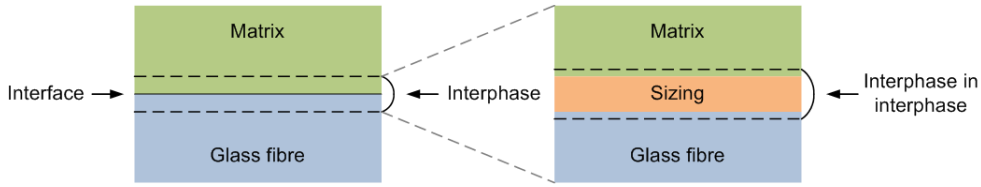

Figure 2.7: Defining the areas of interface and interphase.

The sizing is as mentioned earlier a complex composition where the two main components are film former and coupling agent. The performance and reactions of sizing at the interface is poorly understood. Experience with organosilanes and glass surfaces suggest that a sol-gel reaction can take place and covalently binding the silane coupling agent to the fibre surface. If the functionality of the organosilane is chosen to fit with the matrix it is believed possible to create a connection between the glass fibre surface and the matrix polymer. Even without the bond to the matrix it is suggested that a interpenetrading network is created as illustrated in fig. 2.8 [16, 21]. However as the film former make up around 80 wt.% of the sizing it is likely to take up much more space than illustrated.

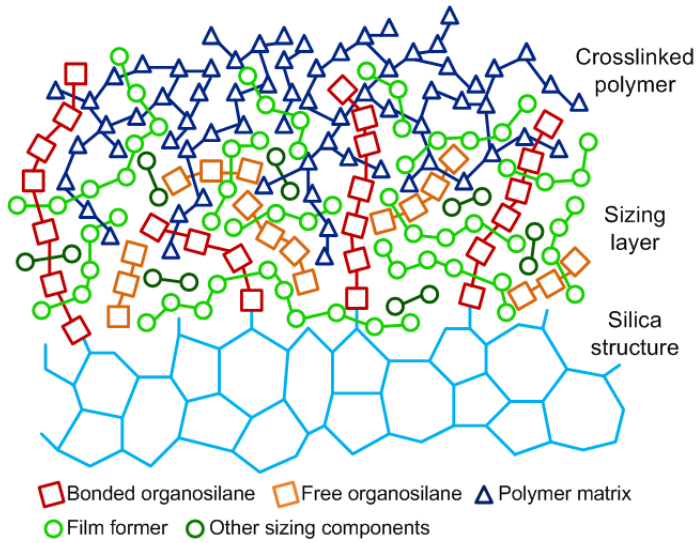

Figure 2.8: The interpenetrading network structure of the interface: glass fibre-sizing-polymer matrix.

2.6 Mechanics of the interface

The two main parameters in mechanics of materials are stress and strain. Stress is the force applied per area and strain is the deformation. The stress can be applied in three ways: tensile, compression, and shear related to the direction of the force. Stiffness and strength are terms, that can be obtained from analysing the deformation of a material, as a function of the applied force. The stiffness is a measure of a materials ability to resist deformation, when exposed to

a force. The strength is the amount of stress applied on a material at the point of failure. The shear strength is the stress coplanar to the cross section of the material, in fibres that is along the fibre surface.

The stiffness of the composite depends very much on the fibre stiffness, since the matrix stiffness is a fraction of the stiffness of the fibres. A strong interface for the stress transfer is therefore desirable. When a force is applied to a composite, the deformation of fibres differ from the deformation of the matrix; due to the mismatch of stiffness. This results in shear stresses (τ_s) at the interface.

In section 1.2 the expressions strong and weak interface is presented. This refer to the adhesion and stress transfer between fibre and matrix where Interfacial Shear Strength (IFSS) is an often used measure of this. The stress transfer across the interface, induces shear forces at the interface which is equal for both fibre and matrix when loading in the fibre direction [4], see fig. 2.9.

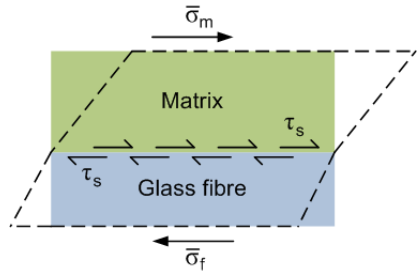

Figure 2.9: Stress transfer between glass fibre and matrix.

3 Materials and Equipment

The materials and equipment used during experiments described in the later chapters are detailed listed in this chapter.

3.1 Materials

3.1.1 Glass Fibres and Plates

- **Fibre A**: E-glass fibres produced by Jushi (Chengdu, China), sizing 320, tex number of 1200, 17 μm diameter of monofilament, moisture content $\leq$ 0.10% and sizing content in the range of 0.45-0.70%
- **Fibre B**: ECR-glass fibres produced by Owens Corning (Brussels, Belgium), sizing SE1500, a tex number of 1200, a diameter of 17 μm.
- **Fibre C**: boron free E-glass fibres supplied by Owens Corning(Brussels, Belgium), sizing APTMS, average diameter of 17.5 μm.
- **Plates**: Plain Micro Slides, 2947-75$\times$25, from Corning Incorporated, USA
- **UD650** A UD fabric without backing (UD650) produced by Jushi from their Jushi-320 E-glass rovings (Chengdu, China) with a fabric area weight of 650 g/m^2, 1200 tex rovings with a fibre diameter of 17 μm, and sizing and moist content of 0.45-0.70 wt.% and $\leq$ 0.10%, respectively.
- **UD950** The filling UD fabric with backing (UD950) produced by Saertex (Saerbeck, Germany) with a fabric area weight of 950 g/m^2 made from 2400 tex rovings.

3.1.2 Matrix systems

- **Epoxy matrix 1**: Araldite 506 (poly(bisphenol-A diglycidylether) resin modified with a monofunctional reactive diluent (butyl glycidyl ether)) and triethylenetetramine (TETA, technical grade 60%) curing agent both from by Sigma-Aldrich, Germany.
- **Epoxy matrix 2**: Araldite LY 1568 (modified low viscosity bisphenol-A based liquid epoxy resin) with Aradur 3489 (aliphatic polyamine) produced by Huntsman Advanced Materials. The stiffness of the matrix is 3.1 GPa when cured as described in 6.2.1.

3.1.3 Other materials

- **APTMS** ((3-aminopropyl)trimethoxysilane), 97%, 1.03 g/cm^3) from Sigma-Aldrich (Steinheim, Germany)

- **GPTMS** ((3-glycidyloxypropyl)trimethoxysilane) ($\leq$ 98%, 1.07 g/cm^3) from Sigma-Aldrich (Steinheim, Germany).

3.2 Equipment

3.2.1 Analysis

- **ATR-FTIR** (Attenuated Total Reflectance Fourier Transform Infrared) spectroscopy was conducted on a Perkin Elmer spectrum 100
- **Contact Angle Measurement System** CAM100 from Crelab Instruments AB (Billdal, Sweden)
- **DSC**(Differential Scanning Calorimetry) performed on a TA Q20 using aluminium pans from TA Instruments (New Castle, United States)
- **Gas Pycnometer** Ultrapyc 1200e from Quantachrome (Hartley Wintney, United Kingdom)
- **TGA-MS** (Thermo-gravimetric Analysis with subsequent Mass Spectrometry) analysis was conducted on a STA 409 CD with a QMS 403 D connected, both from Netzsch (Selb, Germany)

3.2.2 Characterisation

- **Archimedes setup** Density Kit from Mettler Toledo (Greifensee, Switzerland)
- **Inverted Microscope** Olympus GX51 Inverted Metallographic Microscope from Olympus (Tokyo, Japan) with an Infinity 1-5 microscope camera from Lumenera (Ottawa, Canada)
- **Microscope setup with xyz board** Infinity X32 with Navitar adapter (x1) and optic (x2). Motor control of board: Prior, Optiscan II. Software: Deltapix InSight. All from DeltaPix (Smørum, Denmark)

3.2.3 Testing

- **Instron 3342** tensile tester (Instron, Great Britain)
- **Single Fibre Tensile Tester** Favimat+ with a Robot2 from Textechno (Moenchengladbach, Germany)
- **TMA** (Thermal Mechanical Analyser) used was a Q400EM with a MCA70 cooling accessory and an expansion probe mounted all from TA Instruments (New Castle, United States)
- **Load Motor Control of DCB rig** JVL Step Motor Controller SMC35, Birkerød, Denmark
- **Load amplifier** P-3500 Strain Indicator from Vishay Measurements Group (Raleigh, North Carolina, United States)
- **LVDT** linear-variable differential transducer, Type UCA 5C from H.F. Jensen (København, Denmark)

4

Characterisation of sizing and glass surfaces

Sizing is applied directly on the glass fibres. It is therefore rational to begin the sizing analysis with the glass fibre surface. Mainly infrared spectroscopy is used for the analysis. The chapter is divided into two sections, the first concerns the analysis of commercial glass fibres and the second is about mimicking the glass fibre surface on a planar glass surface. The first section is based on results presented in Paper I and further extended by including a comparison of two different types of fibres. The second section consists of unpublished work.

4.1 Removal and analysis of sizing from glass fibres

In literature regarding sizing it is often mentioned that the silane coupling agent reacts with the glass fibre surface whereas the rest is merely physisorbed to the surface. Extraction of non-bonded components in combination with burning has given indications that part of the sizing is neither extractable nor removable by burning as illustrated in fig. 4.1. In the following experiment extraction was used to remove the sizing for further analysis by both infrared spectroscopy and thermal decomposition. It is attempted to characterise the sizing in order to know which functional groups are present at the surface and to distinguish between two different types of fibre and furthermore to investigate the changes of the surface as a function of removing the sizing.

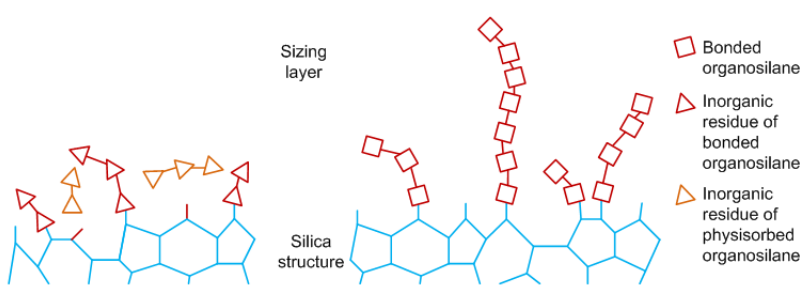

Figure 4.1: Simplified structure of the glass fibre surface after removal by extraction (right) and burning (left).

4.1.1 Methods

The analysed fibres are Fibre A and Fibre B. Sizing was removed by soxhlet extraction and/or by burning. Fibres and sizing extract were analysed with ATR-FTIR and TGA-MS.

The removal of sizing can be performed by different procedures; burning and washing are the most common ways [10, 22]. Soxhlet extraction is a form of washing procedure that separates fibre and extract without destroying the sizing [16]. Heat treatment at 550 °C oxidises organic matter to gasses in the for of CO_2 and H_2O, leaving inorganic residue but it has the disadvantage that the fibres become more fragile than before as it is no longer protected against water by the silane coupling agent [23], see fig. 4.1. The effect of removing sizing by both extraction and burning on strength and stiffness will be investigated later in chapter 6.1.

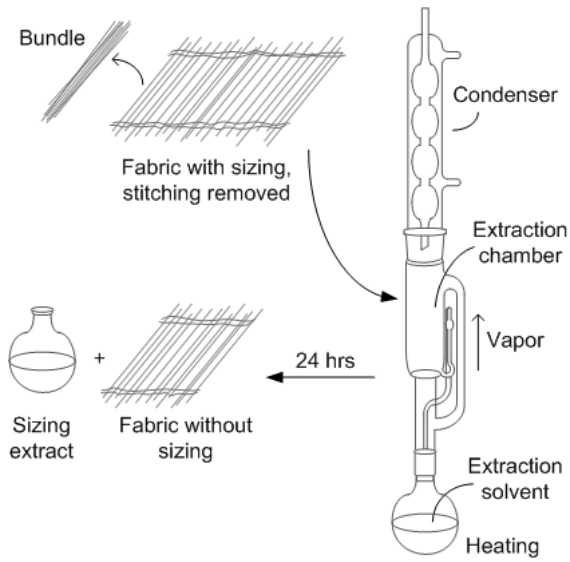

Figure 4.2: Schematic overview of the removal procedure by soxhlet extraction.

The procedure of removing the sizing by soxhlet extraction was mainly based on the work of [22], other studies have used similar removal procedures [9, 23–26]. The schematics of the soxhlet extraction is displayed in fig. 4.2. The fibre samples were around 10 cm long and approximately 10 grams of fibre roving. The extractions were conducted in 200 mL acetone for 24 hours after which they were dried at room conditions for at least 24 hours. Acetone is assumed to only dissolve the sizing components and not react with them during the extraction process. The weight of the fibre samples were determined before and after extraction to calculate the amount of sizing removed. The sizing extracted into acetone was concentrated to a volume of around 20 mL by evaporating acetone. The extraction was repeated three times.

Approximately 10 grams of fibre roving was used for burning off the sizing. The fibres were placed in annealed crucibles at room temperatures in a vacuum oven over night to remove moisture before burning of the sizing. The burning of fibre samples was conducted at 565°C for 3-4 hours. The burn off experiment was repeated three times, each time with five samples.

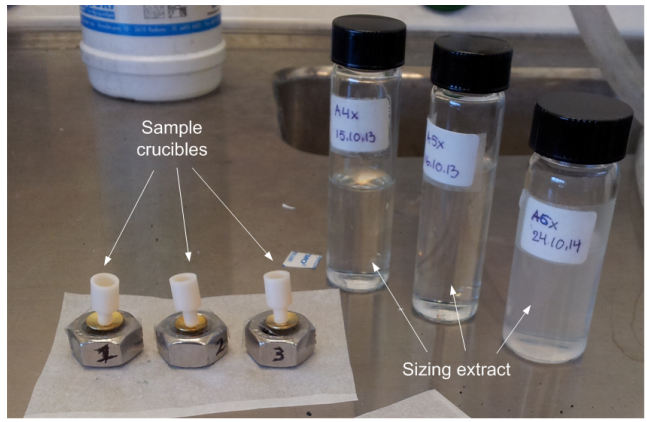

Figure 4.3: Preparation of sizing extract samples for TGA-MS.

ATR-FTIR spectroscopy was conducted from 4000 to 800 cm^{-1} with a resolution of 4 cm^{-1} and 16 scans per sample. Before analysing sizing extract the remaining acetone was removed directly on the ATR crystal by letting it evaporate. Fibre samples were pressed onto the crystal prior to the analysis.

The fibre samples for TGA-MS were cut to a length of 2-3 mm and approximately mass of 100 mg. Sizing extract samples were prepared by evaporating the acetone. One drop was added at the time to the sample crucible until a mass of around 14 mg was reached. The samples were analysed in air using a heating rate of 10°C/min until 600°C was reached. The sizing extract samples can be seen in fig. 4.3.

4.1.2 Soxhlet extraction and burning

The mass losses obtained from the extraction and burning experiment are illustrated in fig. 4.4. The amount of sizing removable by burning found on the commercial fibres Fibre A and Fibre B were within the broad range of 0.2-2 wt.% listed in liteature [10, 27].

Measured values of the extractable part of the sizing exhibited a much wider scatter in the results than the results obtained by burning. This causes the range of extractable sizing to be very wide 65-95 % and 85-92 % for Fibre A and Fibre B, respectively, calculated as the mass loss after extraction compared to the mass loss after burning. This way of calculating the extractable part of the sizing correspons poorly with the residues expected from fig. 4.1, as different parts of the sizing would be left at the glass fibre surface. Instead the extractable part could be calculated from the mass loss obtained by burning after extraction. When the fibres after extraction were burned additional mass losses of 0.07 % and 0.14 % of Fibre A and Fibre B, respectively, were achieved. Using these mass losses to calculated the extractable part yields the ranges 85-90 % and 75-77 % for Fibre A and Fibre B, respectively. The mass losses of Fibre A and Fibre B are very similar both after burning and after extraction. The exception is the mass loss obtained by burning of fibres after extraction of sizing where Fibre A yields a mass loss of half the amount obtained with Fibre B. The silane coupling agent is the only compound that is expected to have the ability to make a covalent bond to the surface. Fibre B exhibits higher amount of sizing that is non-extractable but removable by burning indicating that it has a higher amount of bonded sizing.

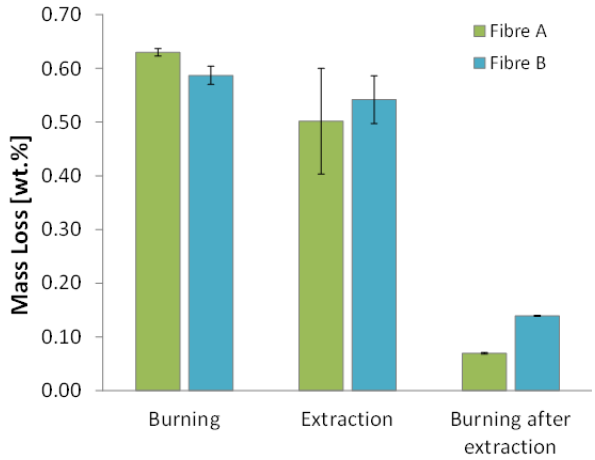

Figure 4.4: Mass losses of Fibre A (green) and Fibre B (blue) after extraction and/or burning. The mass losses are displayed with 95 % confidence intervals.

The film former is extractable and the main part of sizing. In literature film former is indicated to make up around 80 wt.% of the sizing [9], which is similar to the ranges of extracted sizing found on Fibre A and Fibre B. The wide ranges of extractable sizing could be explained by the sizing application method which yields a very uneven distribution of sizing of 1nm-1μm along the fibres [6, 19, 21]. The sizing is transferred rapidly by contact with a roller carrying the sizing suspension. Afterwards the fibres are handled while still wet, enabling that the sizing could wear off, yielding spots with less sizing. As the fibre samples were less than 10 cm, it is possible that this wear off; explains the wide range. The amounts of removable sizing were used to calculate an average thickness of the glass fibres. The density of the glass fibres and of the sizing were assumed to be 2.55 g/cm^3 [5, 21] and 1 g/cm^3, respectively. The sizing density was based on the densities of the organosilanes APTMS and GPTMS. These values yield an average thickness of 60-70 nm which falls within the broad range given above. For comparison the length of the silanes APTMS and GPTMS are around 0.8-1.1 nm.

4.1.3 FTIR analysis

The surfaces of Fibre A and B were analysed using FTIR before and after extraction and burning. Additionally, the sizing extract was also analysed. The spectra displaying the pristine Fibre A and Fibre B can be seen in fig. 4.5.

The spectra are shown both as relative transmittance and with the signal enhanced $\times$20. A brord high intensity band covers the area 800-1200 cm^{-1} making it very difficult to identify bands with a low signal intensity compared to this. The predominant band is associated with Si-O-Si bonds in the glass [28]. The difference in signal strength can be explained by the penetration depth of the infrared light of ($\sim$1 μm) which is much higher than the estimated thickness of the sizing layer. The spectra of Fibre A and Fibre B are almost identical and display no significant difference besides a weak band at 3745 cm^{-1} in an area with a high noise level. The spectra of the fibres after extraction and burning as well as the sizing extract

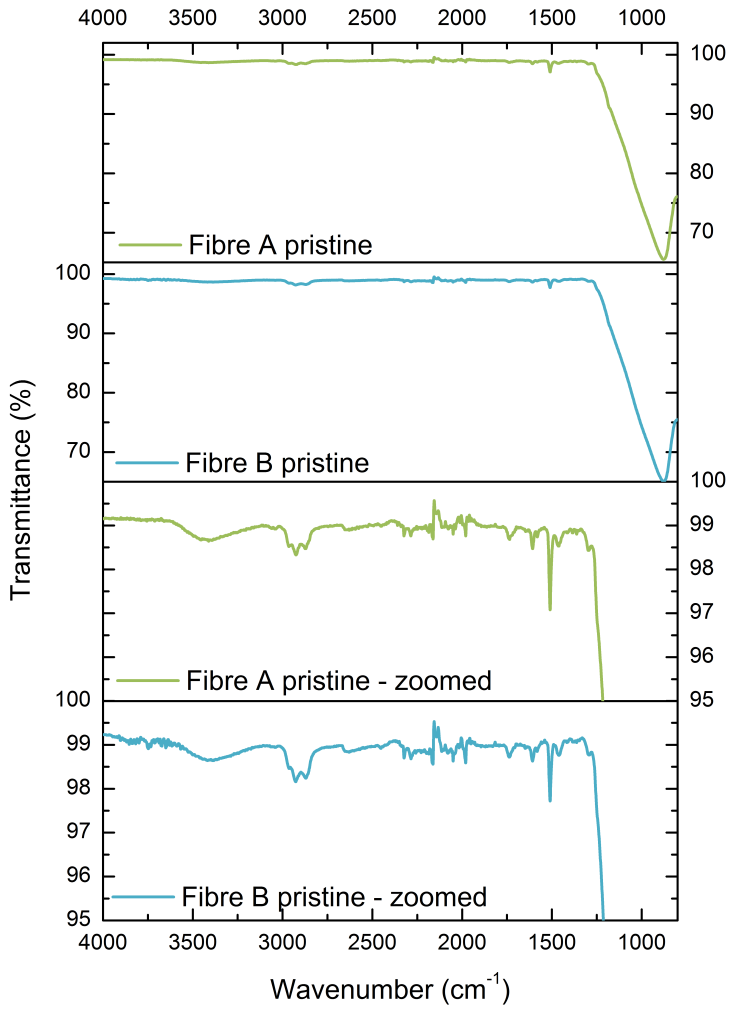

Figure 4.5: FTIR spectra of pristine Fibre A (green) and Fibre B (blue). Note the different scales. Adapted from Paper I.

from Fibre A is displayed in fig. 4.6. The equivalent results from the analysis of Fibre B is not displayed as they are similar to to the ones from Fibre A in fig. 4.6

The spectra of fibres after removal of sizing by extraction and burning both demonstrate only one band dominating the range of 800-1200 cm^{-1} associated with Si-O-Si, see fig. 4.6 C and D. The lack of other bands indicates that the sizing has been completely removed or reduced to an amount below the detection limit of the equipment. Burned fibres should only be covered with the inorganic part of sizing which can be Si-O from silane coupling agent, but is indistinguishable from Si-O in the glass fibre. Furthermore it is not possible to distinguish silane from physisorbed or bonded organosilane.

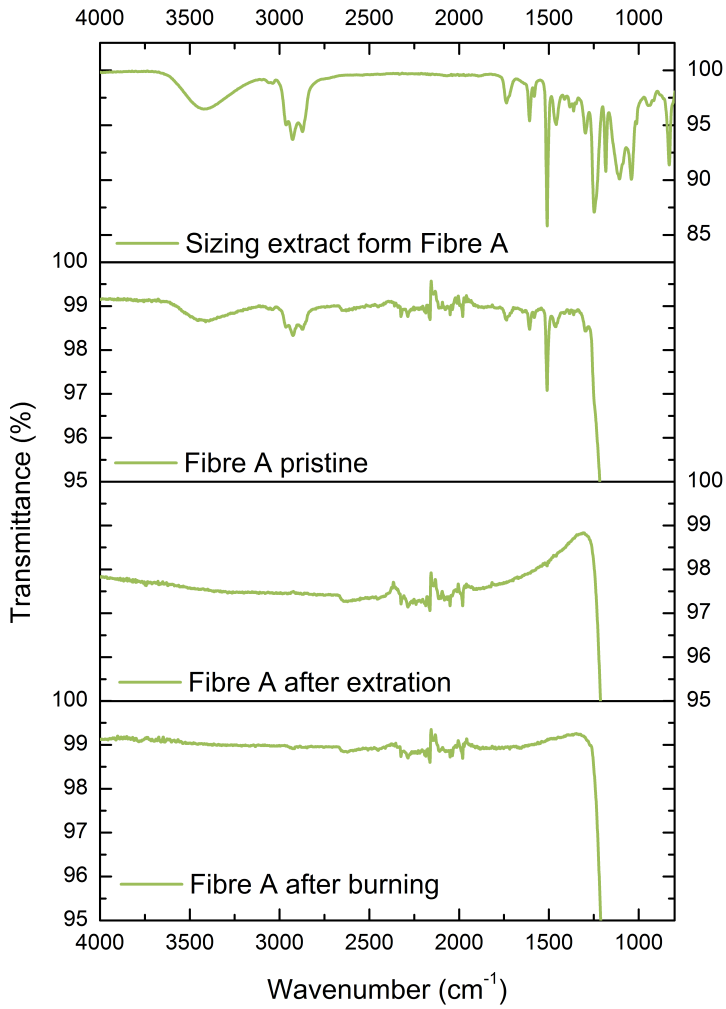

Figure 4.6: FTIR spectra of sizing extracted from Fibre A, pristine Fibre A, Fibre A after extraction and Fibre A after burning. Adapted from Paper I.

The bands visible in the spectrum of pristine fibres are all found in the spectrum of the sizing extract, see fig. 4.6. Analysing the sizing extract both enhances the visibility of the bands but also reveals the bands that were consealed by the Si-O-Si band. The correspondance between the bands detected from pristine fibres and from sizing extract supports a successful extraction. Both spectra displayed a broad band at 3200-3600 cm^{-1} assigned mainly to stretching in O-H. Multiple bands originating from stretching in C-H from CH, CH_2 and CH_3 (both aromatic and aliphatic compounds) were detected in the range 2873-2965 cm^{-1} [25, 28–31]. The band at 1735 cm^{-1} was assigned to C=O stretching of esters/carbonyl [29], that usually exhibits a strong band which indicates that here only a very small amount is

present e.g. sulfactant or antistatic agent. The bands around 1100 cm^{-1} can be attributed to stretching in C-O/Si-O bonds which could correspond with different compounds as polyethylene and silicon oxide [28]. The bands at 830, 1040, 1509, and 1608 cm^{-1} have been assigned to C-O-C in oxirane group, C-O-C of ethers, C-C in aromatics, and C=C of aromatic rings, respectively, all of which are related to the epoxy resin DGEBA (Bisphenol A diglycidyl ether) a possible film former [9, 31]. Only the last two bands are visible in the spectra of pristine fibres. The bands at 1183 and 1248 cm^{-1} both relates to an epoxide group as they are assigned to C-H in plane deformation mode and C-O asymmetric stretching, respectively [32]. However it is possible that the band at 1248 cm^{-1} could also originate from stretching in C-O-C from polyethylene glycol [33] or polyethylene oxide which is an often used lubricant/surfactant in sizing [6]. The bands assigned are listed in tab. 4.1.

Table 4.1: Assignments of bands detected on pristine fibres and sizing extract by ATR-FTIR.

Absorption band	Assignment
3200-3600 cm^{-1}	O-H stretching, bonded to C or Si
2873-2965 cm^{-1}	C-H stretching in CH, CH_2 and CH_3 (aromatic and aliphatic)
1735 cm^{-1}	C=O stretching in esters/carbonyl
1608 cm^{-1}	C=C in aromatics
1509 cm^{-1}	C-C in aromatics
1248 cm^{-1}	C-O asymmetric stretching or C-O-C stretching
1183 cm^{-1}	C-H in plane deformation mode
1100 cm^{-1}	C-O / Si-O stretching
1040 cm^{-1}	C-O-C in ethers
830 cm^{-1}	C-O-C in orixane

4.1.4 TGA-MS analysis

The analysis was conducted on both pristine fibres as well as sizing extract. Each sample was analysed three times yielding three identical graphs in regard to peak location. Only one of the three graphs are displayed here. The first derivative was calculated to obtain a more precise identification of peaks for the interpretation. The mass losses of Fibre A and Fibre B as a function of heating are displayed in fig. 4.7. Fibre A and Fibre B both reach a total mass loss of 0.5% with a small tendency that Fibre A has a little more sizing than Fibre B. The total mass loss falls within the range found by the removal burning experiment in section 4.1.2. The graphs follow almost the same decrease in mass as a function of temperature both having a large mass loss at around 300 °C and a second and a third mass loss close together around 450 °C. One difference between the mass losses of Fibre A and Fibre B is that Fibre A loses less mass around 300 °C, but a little more around 450 °C.

The mass losses of pristine Fibre A and sizing extracted from Fibre A are illustrated in fig. 4.8 displaying the first derivative calculated from the mass measured during heating. Both mass loss curves exhibit two main mass losses but for the sizing extract they are shifted to a higher temperature. This shift has been explained in literature by differences in sample size and concentration [29]. The fibre samples have a weight of around 100 mg where the glass fibres are dominant and the sizing extract samples being mere 14 mg but only sizing. An additional factor is the very different surface-volume ratio of the two samples. Also the mass losses behave differently as the two peaks at 420 and 460 °C for the fibre sample corresponds

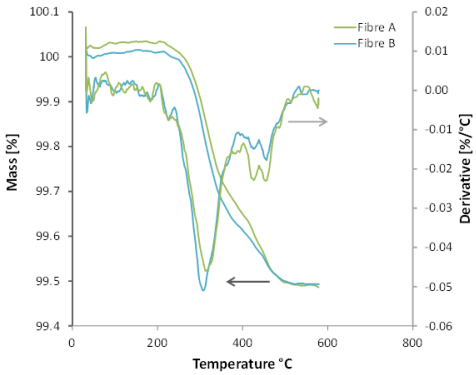

Figure 4.7: TGA mass loss curves of pristine Fibre A (green) and Fibre B (blue) along with the first derivative of the mass loss on a separate axis both as a function of temperature. Adapted from Paper I.

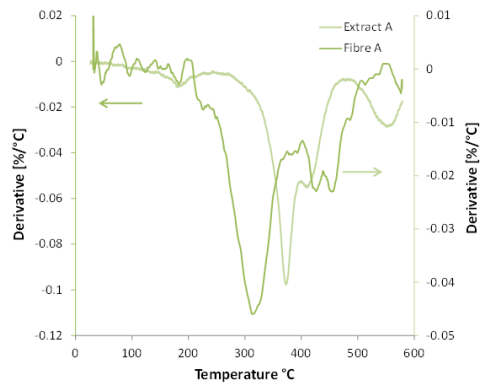

Figure 4.8: The first derivative of the mass loss curves of pristine Fibre A (green) and the sizing extract (light green) from Fibre A on primary and secondary axes displayed against the temperature. Adapted from Paper I.

to a single peak at 551 °C for the extract but where the main peak has a shoulder peak. Despite these differences the mass loss curves are much alike indicating that the sizing analysis is in some degree reproducible, similar deductions have been done in literature [29, 34]. The sizing extract yields almost a 100 % mass loss when the temperature reaches 600 °C. However it might fit well with the last part of the peak around 551 °C being incomplete. Fibre A and the sizing extract both display a small mass loss at 183 °C which is attributed to oxidation of silicon dioxide from the surface of the glass structure releasing water [35].

In fig. 4.8 the dominant mass loss from Fibre A detected at 320 °C covers 63 % of the total mass loss. The additional mass losses observed at 420 °C and 460 °C cover approximately 35 % of the total mass loss. The corresponding values for Fibre B are 76 % at 306 °C and 23 % at the combined peaks at 425 and 456 °C. The graph of sizing extracted from Fibre A in fig. 4.8 displays a major peak at 372 °C with a shoulder peak at 409 °C and an additional peak at 551 °C. The first peak together with the shoulder covers around 67 % of the total mass loss in the analysed temperature interval. The second peak makes up around 19 % of the total mass loss. The distribution between the peaks in the graphs of fibre and sizing extract are similar to the average weight distribution of the two main sizing components where film former and organosilanes account for 79 % and 10 %, respectively [9]. The TGA graph of both fibre and sizing extract displays a second (and third) peak correspond to amounts that exceeds what was expected to originate from the silane coupling agent. The dominant peak at 372 °C in the TGA graph from the sizing extract in fig. 4.8 could originate from a film former polymer and the shoulder at 409 °C might also be a film former polymer as film formers sometimes consist of a mixture of different polymers. The second (and third) mass loss around 450 and 550 °C in the TGA graphs of fibre and sizing extract, respectively, is associated with the sizing fraction covalently bound to the fibres despite that it exceeds the expected 10 %. Comparing the mass loss peaks of Fibre A with the sizing extract from Fibre A in fig. 4.8, the difference in the distribution could be explained by an increase in reactivity as the surface

area of the sizing on glass fibres far exceeds the pure extracted sizing. This can result in an oxidation at lower temperature releasing H_2O, CO and CO_2 gasses.

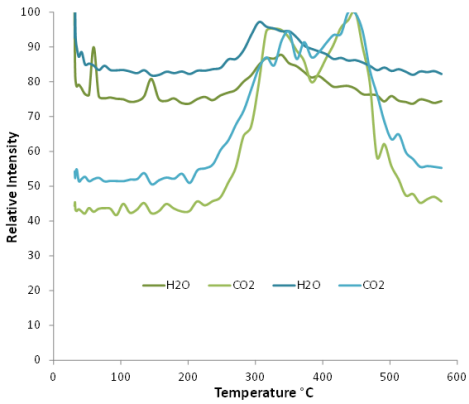

Figure 4.9: MS spectra of pristine Fibre A (green) and Fibre B (blue) displaying m/z corresponding to H_2O (m/z=18) (dark) and CO_2 (m/z=44) (light) as a function of temperature. Adapted from Paper I.

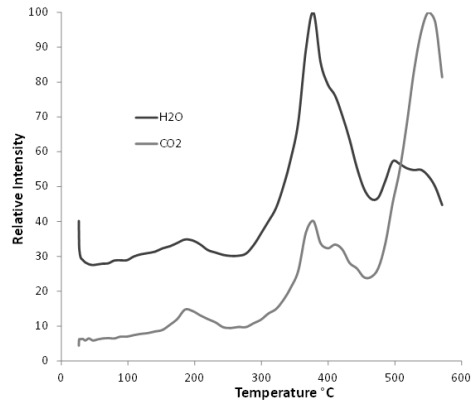

Figure 4.10: MS spectra of sizing extract from Fibre A displaying m/z corresponding to H_2O (m/z=18) (dark grey) and CO_2 (m/z=44) (light grey) as a function of the temperature. Adapted from Paper I.

The spectra of the masses m/z 18 and 44 relate to H_2O and CO_2, respectively, where chosen as a combustion reaction is expected from the presence of organic material yielding a separation of different compounds. The MS graphs of the masses equal to H_2O and CO_2 as a function of the temperature corresponding to the TGA graphs are displayed in fig. 4.9 and fig. 4.10.

The peaks in the MS spectra of Fibre A and Fibre B in fig. 4.9 are similar and match the two mass loss peaks found with TGA. The MS spectra connected to Fibre A and Fibre B fibre samples have a broad peak at approximately 320 °C and 306 °C, respectively, for both H_2O and CO_2 masses. Additionally the CO_2 graph has a broad peak just above 400 °C where no such peak is found in the H_2O graph. This can be due to low sensitivity of the measurement and/or partial oxidation of silicone groups[36]. The MS spectrum of sizing extract in fig. 4.10 displays the presence of H_2O and CO_2 with two main peaks at 372 °C (inclusive a shoulder at 409 °C) and at 550 °C. The intensity of the H_2O peaks found in the sizing extract are clearly different. This intensity difference is opposite for the CO_2 peaks. This indicates that the components degenerating at these temperatures have different compositions.

This was investigated by analysing the MS spectra corresponding to the temperatures at which peaks have been observed distributed on masses, see fig. 4.11. The analysis revealed that the composition was almost the same for each of the temperatures within the same sample besides a higher detection of H_2O at the first peak (306/320 °) for the fibre samples. Fibre A and Fibre B were also not distinguishable from each other. The spectra from Fibre A sizing extract displayed some differences in intensity but the same compounds were detected. Most of the fragments found were small molecules as OH (m/z=17), CHO/C_2H_5 (m/z=29). There were some small indications of benzene derivates that could be related to DGEBA, a possible film former.

4.1.5 Summary

Fibre A and Fibre B contained a reasonable amount of sizing removable by soxhlet extraction compared to values reported in literature for commercial glass fibres [10, 27]. The extractable part makes up around 75-90 wt.% related to the amount removable by burn-off at 565°C after soxhlet extraction, which is similar to literature values as well [10]. The difference in the

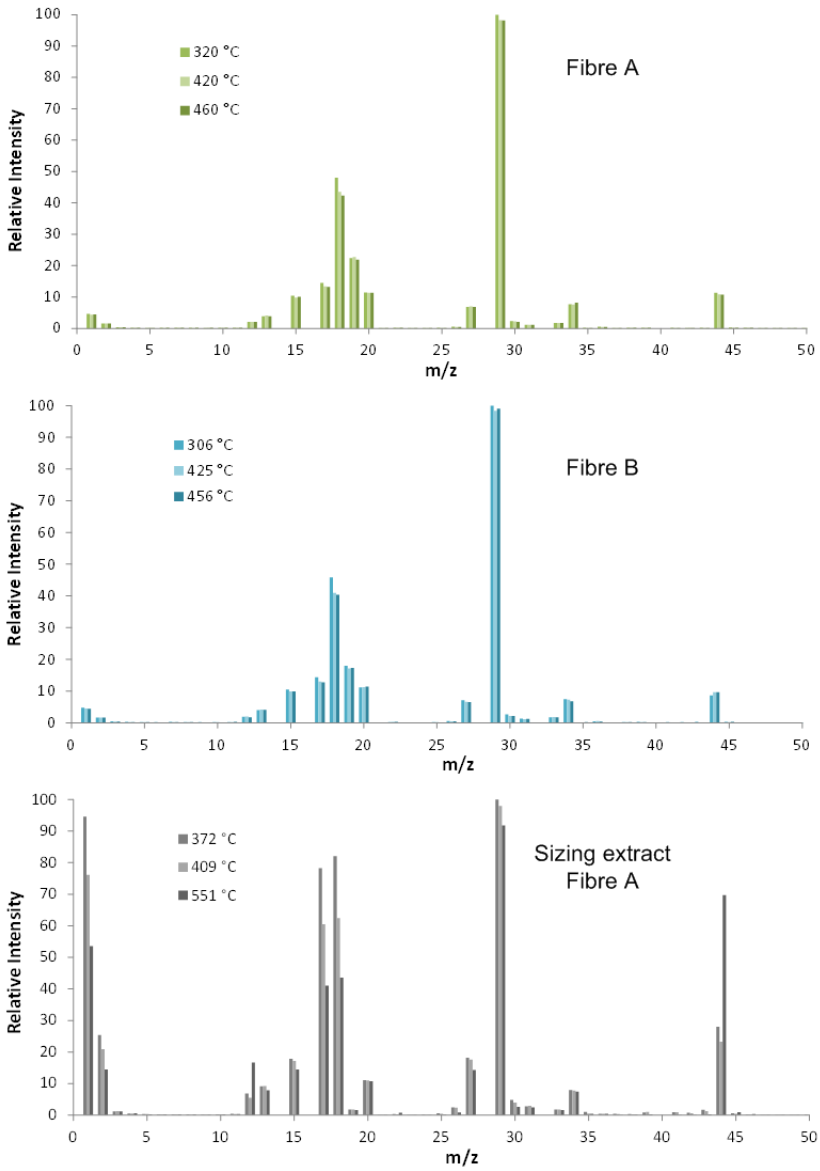

Figure 4.11: MS spectra displaying the relative intensity as a function of masses (m/z) of pristine Fibre A (green), pristine Fibre B (blue) and sizing extract of Fibre A (grey) obtained at different temperatures selected from the TGA results.

amount of sizing removable by burning and by extraction indicates that a part of the sizing is not removable and could be covalently bonded to the glass fibres. The non removable part of sizing might be unevenly distributed along the fibres, expressed by a large variation in the quantity determinations.

It was not possible to distinguish unambiguously between Fibre A and Fibre B with neither FTIR analysis nor by TGA-MS analysis. The observation of IR bands associated with DGEBA gives a strong indication that this epoxy resin is used as film former in the sizing. However the MS spectra only yields small indications of this after combustion. The FTIR analysis also indicated the presence of a polyethylene oxide lubricant and/or surfactant. Analysis by TGA-MS found two major components each with a weight distribution similar to expected values of film former and silane coupling agent indicating that they combust at different temperatures.

4.2 Dip-coating and analysis of glass plates

The cylindrical shape of the glass fibres are not ideal for all analysis methods like contact angle measurements. It is therefore attempted to mimic the glass fibre surface on planar glass plates. Silane coupling agent is included in the sizing partly to protect the surface against water. Glass plates were coated with organosilane and then analysed with infrared spectroscopy and a contact angle study to observe the surface changes.

Literature indicates that organosilanes with an amino or epoxide group are commonly used in sizings for glass fibres aimed for epoxy resin based composites [7]. Glass plates were therefore treated with an amine functionalised (APTMS) and an epoxide functionalised (GPTMS) organosilane to mimic glass fibres coated with only these organosilanes to obtain indications on how the surface of the glass changes. The two organosilanes chosen for dip-coating were also used as references in the IR analysis.

4.2.1 Methods

The glass plates were cleaned prior to the dip-coating either by burning at 600 °C for two hours or by sonication in acetone for 2×5 minutes. The dip-coating was done by submerging the clean plates in a boiling 1 vol.% APTMS or GPTMS aqueous solution for five minutes. The plates were subsequently dried at 130 °C for three hours. Six plates were cleaned by sonication and six plates by burning. Half where coated with APTMS, the other half with GPTMS.

Static contact angles were measured with deionized water and glycerol in air at room temperature on cleaned and coated glass plates using a fixed camera setup. A typical drop size was approximately 1 x 10^{-9} m^3. The contact angle was measured within 10 seconds after the drop had been applied to the plate surface. Dispersive and polar components of the surface energy were obtained by the two-liquid geometric method by solving eq. 4.1 that uses the Lifshitz-van der Walls interaction (γ_S^d) and the electron-acceptor/electron-donor interaction (γ_S^p) [37].

$$(1+cos\theta_i)\cdot(\gamma_{Li}^d+\gamma_{Li}^p)=2(\gamma_{Li}^d\cdot\gamma_S^d)^{1/2}+2(\gamma_{Li}^p\cdot\gamma_S^p)^{1/2} \text{ for } i=1,2 \qquad (4.1)$$

where θ is the contact angle, γ_L^d and γ_L^p are the dispersive and polar components of the surface energy of the used liquids, i denote deionised water (i=1) and glycerol (i=2).

4.2.2 FTIR analysis

FTIR spectra of the analysed plates and references (pure APTMS and GPTMS) are displayed in fig. 4.12. The spectra are all shown in the range of 800-1800 cm^{-1}. The spectra from analysis of the glass plates exhibit strong absorption from Si-O-Si bonds which obstruct other signals in the area around 900-1100 cm^{-1}. The Si-O-Si bonds give rise to a high and broad band since the amount of glass is much higher than the one of applied organosilane. Plates cleaned by either burning or sonication were also analysed but both displayed only the broad Si-O-Si band with no apparent difference between the two cleaning methods. The spectra of coated plates exhibited only few bands above 1800 cm^{-1}; the multiple bands originating from stretching in C-H of CH, CH_2 and CH_3 (in aromatic and aliphatic compounds) at 2965-2873 cm^{-1} were detected [25, 28–31]. The characteristic epoxy band at 916 cm^{-1} was only visible in the spectrum of pure GPTMS [36]. Bands associated with epoxide (1248 and 1183 cm^{-1}) [32] were observed in the spectra of plates dip-coated with GPTMS, but at a little higher wavelength: 1255 and 1200 cm^{-1}. These bands are slightly shifted compared to the GPTMS reference. Also the plates dip-coated with APTMS exhibits bands that are slightly shifted compared to the APTMS reference: 1580 and 1475 cm^{-1} which were assigned scissor vibration in N-H and deforming vibration in CH_2-NH, respectively. The spectra of pure APTMS and plates coated with APTMS also displayed two bands at 3280 and 3350 cm^{-1} associated with stretching in NH_2. The spectrum of plates coated with GPTMS exhibited a strong broad band around 3200-3600 cm^{-1} assigned OH stretching from hydrolysis of alkoxy groups [21]. Both the APTMS and the GPTMS references display a very strong broad band with centre around 1070-1080 cm^{-1} which seems to have shifted to 1100-1125 cm^{-1} for the coated samples. The bands are less visible as the large band from absorption of the Si-O-Si bonds covers this range. The shifting of some of the bands detected on the coated plates could indicate that the organosilanes are not just physisorbed to the glass surfaced but possible bonded.

4.2.3 CA analysis

The surface of the glass plates, both cleaned and coated, were analysed by measuring the angle between a droplet and the glass plate surface. In tab. 4.2 the results from the measurement of contact angle with both droplets of water and glycerol are listed along with the surface energy components.

The water contact angle was 18° on the plates cleaned by sonication whereas the angle where not possible to obtain of the plates that had been burned at 600 °C since the droplet flattened beyond measuring. This show a clear difference between the cleaned surfaces that was not detected by the FTIR analysis. After the silane treatment the water contact angle increased considerably to a level of 64-92° depending on the organosilane and the cleaning method. A similar tendency was recorded with glycerol contact angles, but to a less extend.

The polar component of the surface energy of the plates changed drastically after being treated with either GPTMS or APTMS where the change in the dispersive component was to a lesser extent. As a result the total surface energy decreases significantly from 72 to around 24-38 $mJ{\cdot}m^{-2}$ after treatment. Comparing the two treatments the APTMS treatment shows in general slightly higher contact angles, with the largest difference between the plates that had been cleaned by burning prior to the treatment. Furthermore, the plates treated by the same organosilane exhibit a clear difference depending on the cleaning method. The contact angle increase is highest for the sonicated plates. All in all is the largest increase in contact

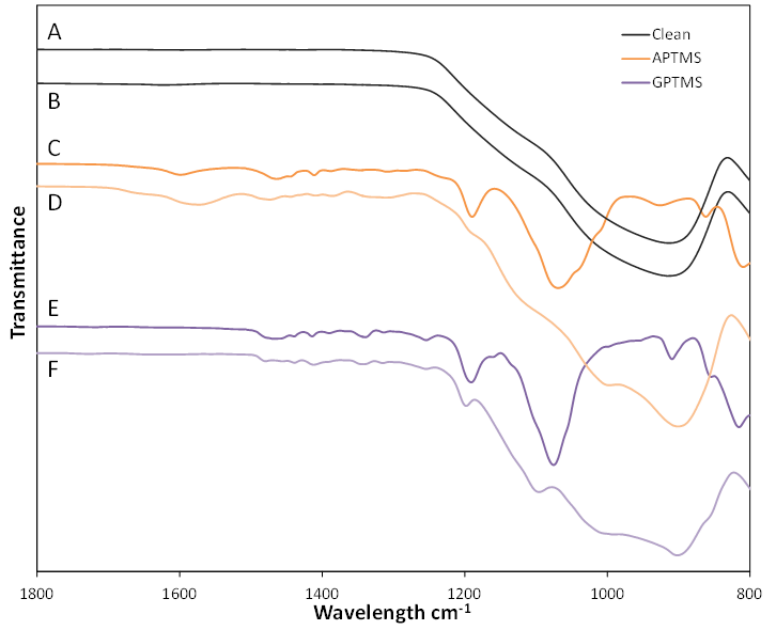

Figure 4.12: ATR-FTIR spectra of plates A) cleaned by burning and B) by sonication, and plates dip-coated with D) APTMS and F) GPTMS after they have been cleaned by burning. The spectra of the pure organosilanes used for the dip-coating are also displayed as references C) APTMS and E) GPTMS. Note the different scales.

angle and decrease in total surface energy was found with plates cleaned by sonication and treated by APTMS.

Table 4.2: Water contact angle and dispersive and polar components of surface tension of glass plates. The glass plate samples were dip-coated with APTMS or GPTMS using plates that had been cleaned by burning at 600 °C or by sonication in acetone. Three samples for each cleaning and treatment.

Cleaning	Sonicated			Burned	
Treatment	Clean	APTMS	GPTMS	APTMS	GPTMS
Water contact angle [°]	17.8 ±4.0	91.5 ±2.9	80.3 ±2.9	84.5 ±2.9	63.5 ±10.2
Glycerol contact angle [°]	21.2 ± 1.7	80.9 ±1.5	71.1 ±5.8	74.4 ±1.7	59.8 ±11.7
Dispersive component of surface energy [mJ·m^{-2}]	10.7	19.3	18.8	18.8	11.7
Polar component of surface energy [mJ·m^{-2}]	61.1	4.4	9.7	7.8	26.3
Total surface energy [mJ·m^{-2}]	71.8	23.6	28.6	26.6	38.1

4.2.4 Summary

The analysis of dip-coated plates by ATR-FTIR confirmed that the two organosilanes were deposited on the plates. Some of the band reference values for the organosilanes were slightly shifted after being dip-coated onto glass plates which can be explained by a change in the bonds or perhaps due to the major presence of Si-O bonds from the glass interfering with the measurement.

The contact angle measurement of the dip-coated glass plates showed drastic changes. The treatment gave rise to a change in surface energy and mainly in the polar component. From this it is deduced that the chemical change in the glass surface also changes the surface to be more polar. A more polar surface could increase the wetting of the glass surface by a polymer matrix.

5

Investigation of the glass fibre/epoxy interface by microbond testing

The next step of analysing the sizing is to observe its impact on the interface between glass fibre and polymer matrix. Microbond testing investigates samples consisting of a single fibre embedded in a droplet which can be considered as a model of the smallest unit of an actual composite. The present chapter covers an analysis of how the matrix composition and the temperature affect the interfacial shear strength determined by microbond testing. The chapter is based on results presented in Paper II and Paper III.

5.1 The interfacial shear strength and adhesion

The interafacial shear strength (IFSS) is often used as a measure of the adhesion between two materials. When investigating the adhesion between fibres and a matrix polymer of composites different micromechanical methods can be used to determine the IFSS e.g fibre pull out, single fibre fragmentation and microbond testing. The microbond test itself is not a standard method, so it differs from laboratory to laboratory [38]. Until a standard way of determining IFSS is established it is nearly impossible to compare the results obtained from different studies [39]. Here the microbond test will be used in two different setups testing, samples manufactured via the same procedure in order to make a meaningful comparison of the results.

The sizing constituent silane coupling agent is often an organosilane functionalised with an amine or an epoxide group. Consequently the ratio between amine:epoxide must be different at the interface. In epoxy matrices both of these groups are present and reacting in order to create the crosslinked polymer, that yields the desired rigid structure, see section 2.2. It is of interest to investigate the effect of changing the chemistry of the sizing on the IFSS. This can be troublesome to do without an industrial partner [15], since it is difficult to produce fibres with different sizings in the laboratory both in regard to constituents and to concentrations at the same conditions, as when they are manufactured in the industry. A way to get around the issue is to change the matrix material instead. In epoxy polymers this can be done fairly easy by shifting the ratio between epoxy resin and curing agent. Thus in this experiment different ratios of amine:epoxide in the epoxy polymer will be tested, to investigate if the amount of amine groups from the sizing may affect the ratio at the interface, and hereby affect the IFSS.

Altering the ratio between amine and epoxide groups affects more than just the crosslinking structure. The glass transition temperature is another important parameter. It marks the temperature at which a material changes from the glassy state to a viscous/rubbery state. The

glass transistion temperature is located below the melting temperature of the solid material and marks a change in the structure and mechanical properties of the material. The IFSS have been shown to be affected by the temperature at which the testing was conducted especially around the glass transition temperature [40]. Consequently the experiment also include varying the testing temperature; in a range around the glass transition temperature.

5.1.1 Methods

The fibres used in the following analysis were Fibre C and the Epoxy matrix 1. Fibre C was sized only with an amino functionalised silane. No film former or other components that could interfere with the amine:epoxide ratio at the fibre-matrix interface were present. Two microbond setups were used, an Instron tensile tester and a TMA. The Instron microbond setup can be seen in Paper IV. The first for testing at room temperature and the later for testing at specific temperatures in the range of 20-120 °C. Each sample was measured using the image processing program ImageJ on images obtained with an inverted microscope with a magnification of 200, see fig. 5.1.

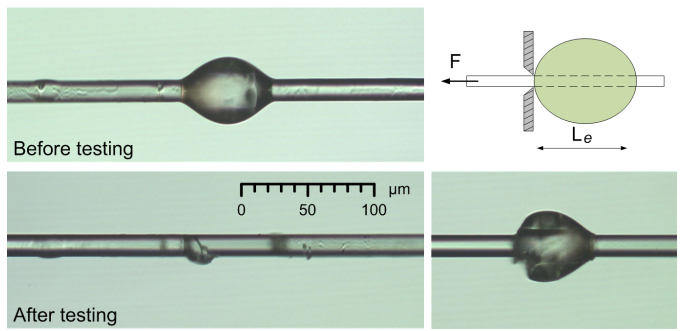

Figure 5.1: Images of a epoxy droplet on a glass fibre before and after microbond testing. The droplet after testing was found further down the fibre hence the two images. The images were obtained with a inverted microscope. An illustration of the debonding is included. The embedded length is marked.

Microbond samples

Epoxy resin and curing agent were mixed in different ratios calculated according to the ratio between amine and epoxide groups. The stoichiometric ratio is 1:1 which is equivalent to 12 wt.% TETA for the present epoxy system. This was calculated based on the equivalent weight of epoxide groups (172-185 Da) and the molecular weight of the hexafuncionalised TETA (146.23 g/mol). Approximately 1-2 g of epoxy resin was used for each batch where the amount of curing agent differed. Ten batches were made for the Instron microbond samples in the amine:epoxide ratio range of 0.1 to 2.5 equal to 1-34 wt.% TETA. Seven batches were made for the TMA microbond samples in the ratio range of 0.5-2.1 equal to 6-22 wt.%. The epoxy resin and curing agent were mixed thoroughly and degassed under vacuum for minimum 12 minutes. Droplets were deposited on single glass fibres fixated in cardboard frames, see fig. 5.2. The frame ensures a gauge length of 5 mm for all the samples. A hole was punched in the cardboard for the Instron microbond setup as can be seen in fig. 5.3. The samples for the TMA microbond setup were cut to fit inside the TMA probe, see fig. 5.9. A

minimum of 60 samples were made for each of the ten different amine:epoxide ratios used for the Instron microbond setup. 30 TMA microbond samples were made for each of the seven ratios and four testing temperatures. The samples were cured in a convection oven with the following curing cycle: from room temperature to 60 °C, with a heating rate of 2 °C/min, kept isothermally for one hour then further heated to 120 °C with a heating rate of 2 °C/min, where it was maintained for two hours. Afterwards the samples were left to cool over night.

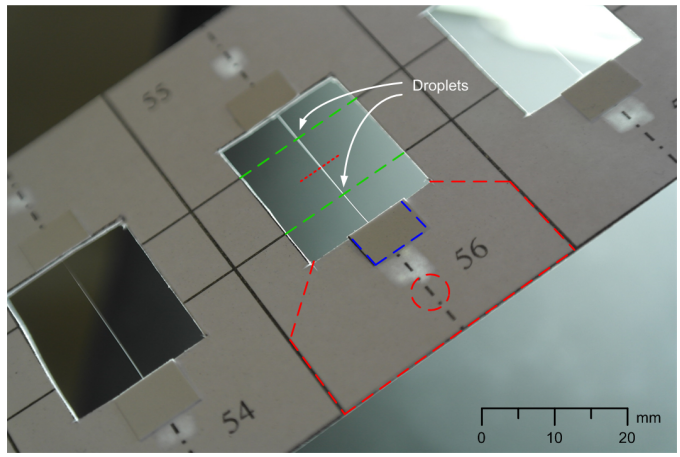

Figure 5.2: A row of cardboard frames. Each frame contains two samples when cut into half. The green lines across the frames mark where the droplet is applied. The red lines mark the sample for the Instron microbond setup. The blue lines mark the TMA microbond sample.

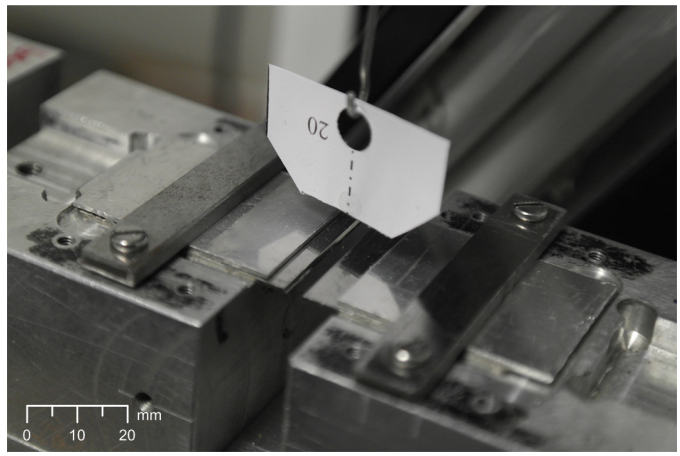

Figure 5.3: Close-up of a microbond sample in the fixture for the Instron microbond setup.

Microbond test

Prior to the testing each sample was measured by image analysis to obtain values of fibre diameter and the length of the fibre covered by the droplet. The apparent IFSS was calculated from these values together with determinations of the maximum load, see eq. 5.1. The shear along the interface is assumed constant. In the following the apparent IFSS will be denoted IFSS.

$$\mathrm{IFSS} = \frac{\mathrm{F}_{max}}{\mathrm{A}_e} = \frac{\mathrm{F}_{max}}{\mathrm{L}_e \cdot \mathrm{d}_f \cdot \pi} \,, \tag{5.1}$$

where F_{max} is the maximum load, A_e is the embedded area, L_e the fibre length covered by the droplet and d_f is the diameter of the fibre. The embedded length is marked in fig. 5.1.

Both the Instron and the TMA microbond setups have been presented in detail previously [41, 42]. The principle of the microbond test is to pull a droplet of resin off a fibre by tensile loading until the droplet debonds. Knife blades were used in both setups to retain the droplet while the fibre is being pulled. In the Instron microbond setup the blades were movable and a microscope was used to position the blades correctly. The fibre was pulled with a constant strain rate of 0.1 mm/min. In the TMA microbond setup a wedge of two blades glued together was used to retain the droplet while the movable quartz probe pulled the fibre with a constant load rate of 0.15 N/min. The TMA is not manufactured to be used for microbond to which it in this experiment has been exploited for, but rather for determination of the linear coefficient of thermal expansion. This explains why the load is controlled and the extension measured.

Load-extension curves were recorded for both microbond setups, the maximum load was determined from these. The samples were viewed with optical microscopy after testing to confirm the debonding.

5.1.2 The Instron microbond setup

The fixture used is crafted specifically for the Instron microbond setup, see fig. 5.4 and fig. 5.5 [38]. An optical microscope was used for aligning the knife blades to the fibre and to position the droplet by turning the micrometers and adjusting the height, respectively. During testing the load and extension are recorded continuously until debonding of the droplet. The load-extension curves all display the same structure, with a linear loading to a maximum where the debonding leads to an immediate drop in load, see fig. 5.6. After debonding the droplet is pushed along the fibre which results in a small increase of load until a steady state level is reached. Friction between droplet and fibre surface is the cause of this increase of load. The maximum force was determined for further calculations. The seemingly large extension, compared to the droplet size, is mainly caused by extension in the fibre before the droplet starts to debond. As a result the slope of the load-extension curve equals the stiffness of the glass fibre under the assumption that the debonding of the droplet causes no extension. The stiffness and strength of the single glass fibres are investigated in section 6.1.

The embedded area was calculated in eq. 5.1 and displayed against the maximum load determined from the load-extension curves. The results displayed in fig. 5.7 are obtained by microbond testing of the samples from the batch with an amine:epoxide ratio of 0.5. The results followed the linearity defined by eq. 5.1 with a slope equal to the IFSS. In this investigation the IFSS was calculated for each individual sample and not from the slope based on all the samples in order to obtain a 95 % confidence interval of the average IFSS. In fig. 5.8 the average IFSS of all the batches are displayed against the amine:epoxide ratio.

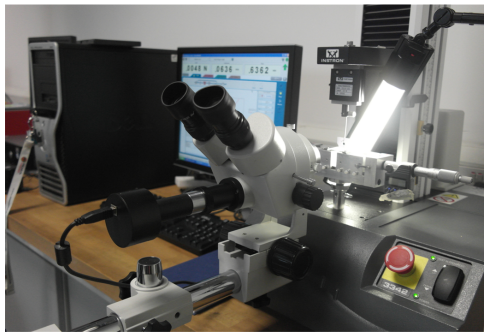

Figure 5.4: The Instron microbond setup: a microbond fixture in an Instron tensile tester with an optical microscope for the allignment of the knife blades.

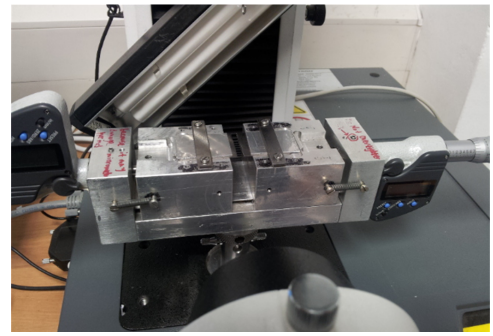

Figure 5.5: The microbond fixture for the Instron tensile tester. The knife blades are moved by turning the two micrometers.

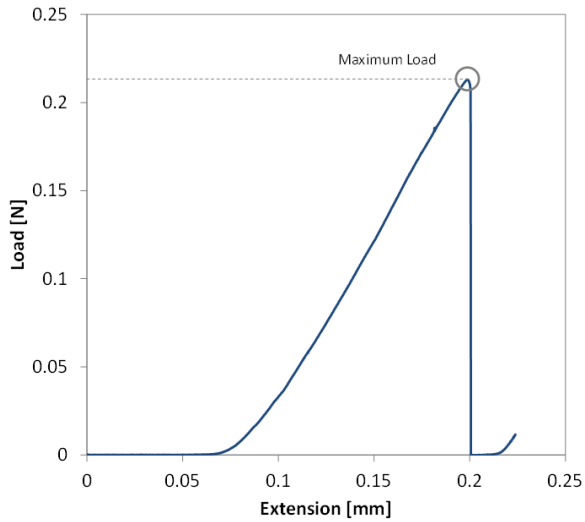

Figure 5.6: Load displayed against extension. The data was obtained by microbond test using the Instron tensile tester. The maximum load is marked.

The IFSS increases with increasing amine:epoxide ratio until a maximum around the stoichiometric ratio is reached after which the IFSS decreases again. The low IFSS values at both high and low amine:epoxide ratios is explained by the material being less crosslinked as it will contain either excess unreacted amine or epoxide groups when moving away from the stoichiometric ratio.

The reactivity of the four amine groups of the curing agent TETA differ as two are primary amines and two are secondary amines, the later being less reactive. Consequently the epoxide groups will react with the primary amines before the secondary. In the case of excess amount of TETA a crosslinking structure will still be the result as long as some of the seconday amine groups react. Since the primary amines in the TETA molecules predominantly react

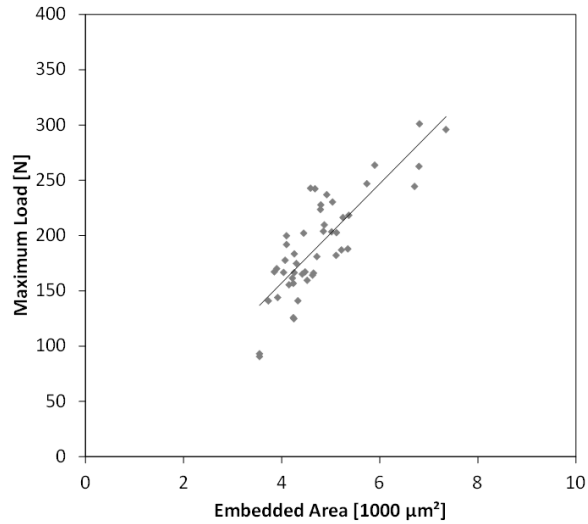

Figure 5.7: The maximum load against the embedded area obtained with the microbond test using the Instron tensile tester at room temperature.

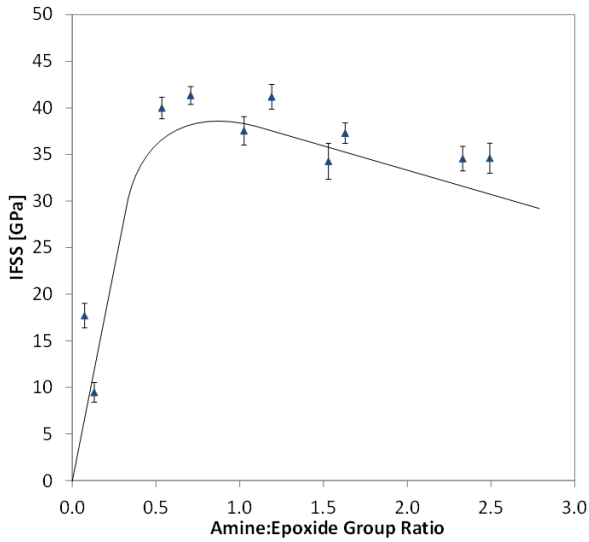

Figure 5.8: The IFSS determined at ten different amine:epoxide ratios at temperature by use of the Instron microbond testing setup. The 95% confidence intervals are displayed for each data point.

before the secondary amines the structure will be less rigid leading to a lower IFSS. With a shortage of amine groups crosslinking is less likely yielding linear polymers as a result [43]. IFSS have been suggested to be related to thermal and residual stresses caused by curing shrinkage as crosslinking obstruct the possibility of relaxing the rigid structure [40, 43–47]. High crosslinking density as found at the stoichiometric ratio of amine:epoxide would then

cause high residual stresses increasing the IFSS [48, 49]. The linear coefficient of thermal expansion also supports a maximum IFSS around the stoichiometric ratio as a minimum was detected as a result of high crosslinking, Paper III. An empirical trendline has been drawn based on the data points in fig. 5.8 and includes the assumption that the IFSS is zero at an amine:epoxide ratio of zero; as the epoxy resin alone is a liquid. The trendline locates the maximum IFSS around the stoichiometric ratio but as a broad curve implying that the maximum could be just below. The results indicate a maximum in an amine:epoxide ratio range of 0.7-1.2.

5.1.3 The TMA microbond setup

The microbond test in the TMA was conducted by sliding in a fibre in the knife blade wedge leaving the droplet ontop and the fibre and cardboard tap below, see fig. 5.9. The loading was accomplished by moving the probe down, retaining the cardboard tap until the droplet debonds. The load-extension curves obtained from the microbond test in the TMA display a different progression than from the Instron microbond setup, see fig. 5.10. The probe moves linear increasing the load rate and as the droplet debonds the resistance drops which results in the probe moving fast downwards to attempt to reach an increase in loading. The extension is measured by the position of the probe. Usually load-extension curves are displayed as load as a function of the extension as most often the extension is controlled and the load measured. Here it is opposite: the extension is measured and the load controlled. For this reason it would make more sense to display the extension as a function of the load as in fig. 5.11 for easier understanding. The high increase of extension with minimal increase in load before and after the debonding is caused by a maximum load speed to avoid destroying the sample. The first part of the extension is the distance from the probe to the cardboard part of the sample. The second increase in extension is where the probe drags the debonded droplet down the fibre.

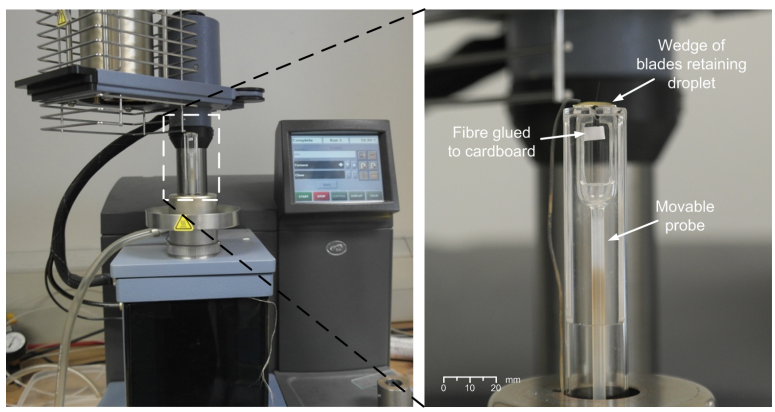

Figure 5.9: The TMA microbond setup.

Using the TMA made it possible to determine the IFSS at different testing temperatures which were selected considering the glass transition temperatures. The glass transition temperature had been determined at amine:epoxide ratios similar to the ones used in this experiment Paper II. The results exhibited a maximum when the amine:epoxide ratio was around the stoichiometric ratio as expected from literature [50]. Four testing temperatures were selected as they were above, around and below the glass transition temperature. The maximum

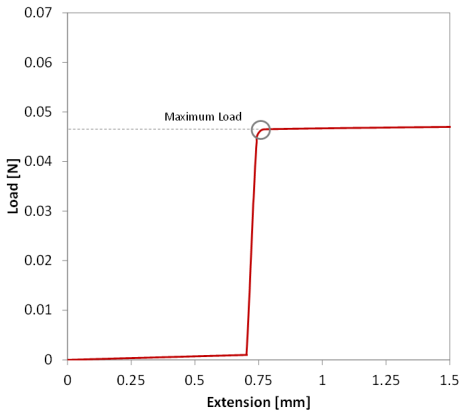

Figure 5.10: Load against extension dataset obtained by microbond test using the TMA. The maximum load is marked.

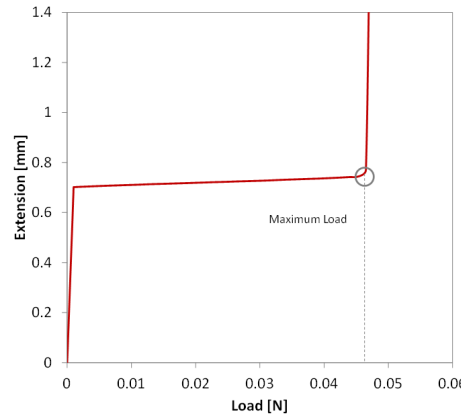

Figure 5.11: Extension against load dataset obtained by microbond test using the TMA. The maximum load is marked.

load results obtained using the TMA microbond setup of the batch with an amine:epoxide ratio of 1.0 is displayed in Fig. 5.12 against the embedded area determined by images of the droplets.

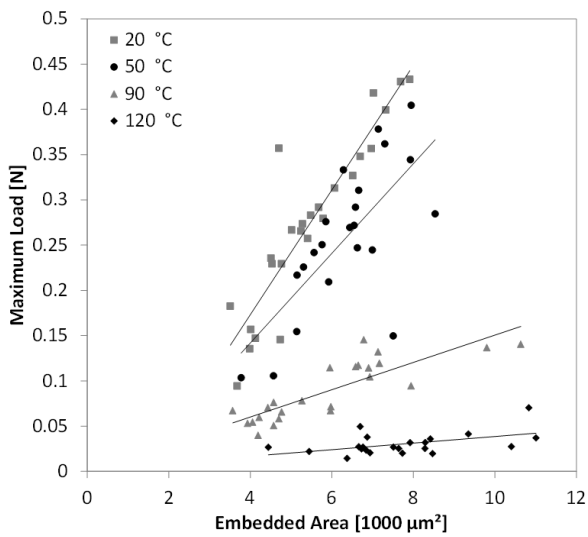

Figure 5.12: The maximum load against the embedded area. Four series tested at 20, 50, 90, and 120 °C all with the same amine:epoxide ratio of 1.0 (the stoichiometric value) using the TMA microbond setup. The trendlines are obtained but linear least squares method.

The maximum load was used to calculate the IFSS in the same way as for the results from the Instron microbond setup using eq. 5.1. Directly from fig. 5.12 it is clear that the IFSS changes as the testing temperature changes. The IFSS increases as the testing temperature

decreases as expected from literature [40, 42, 44, 45], but leaving a clear gab between the two series tested at 50 and 90 °C, respectively. This gab coincides with the glass transition temperature to be in the range of 49-87 °C for the tested amine:epoxide ratios. The gab was also observed at the other amine:epoxide ratios tested, see Paper II where the IFSS results of all seven amine:epoxide ratios are displayed. This indicates that the glass transition is of high importance for the IFSS as the material properties change. However the glass transition temperature might only be part of the explanation of the phenomenon as the same gab is present at the 0.5 ratio having a glass transition temperature of 49 °C.

The TMA microbond testing below the glass transition temperature yielded a progressing of IFSS similar to what was found with the Instron microbond setup in fig. 5.8 whereas the testing above the glass transition temperature resulted in low IFSS and a more linear behaviour without a maximum around the stoichiometric ratio, see Paper II. The IFSS maximum was indicated to be within the range of 0.8-1.0 amine:epoxide ratio by the series tested below the glass transition temperature, with the highest IFSS obtained at a testing temperature of 20 °C. Testing temperatures below the glass transition temperature would not be expected to result in drastic changes in the stresses caused by the rigid crosslinked structure and hereby neither in the IFSS. On the other hand would testing temperatures above the glass transition temperature cause stresses to be relieved reducing the stress and the IFSS [46]. Furthermore internal deformations could result in a higher value of IFSS determined below the glas transition temperature as the deformation would be able to relax at high temperatures [51].

5.1.4 Comparing the two microbond setups

The maximum IFSS was expected to be obtained at or close to the stoichiometric ratio [46] which to some degree was indicated by both the Instron and the TMA microbond testing. Both methods also yielded results following the same behaviour when testing below the glass transition temperature, but when comparing the two methods it is clear that the IFSS determined by the TMA microbond method was around 10 GPa higher.

The difference might be explained by the two ways of loading. The Instron microbond setup loads by constant strain rate where the TMA microbond setup is by constant load rate. As a result the TMA microbond test is conducted much faster leaving less time for deformation increasing the stress at the interface. It seems as the mismatch is constant and in order to investigate this the data were normalised to the maximum value for the results obtained at room temperature, see fig. 5.13. The overlapping of the results is quite convincing indicating that the behaviour is independent of the method.

5.1.5 Summary

The amine:epoxide ratio was found to affect the IFSS to a great extend. The IFSS obtained at testing temperatures below the glass transition temperature progressed towards a maximum around the stoichiometric ratio. The maximum was determined to be in the range of 0.7-1.2 amine:epoxide ratio using the Instron microbond setup. The results from the TMA microbond testing yield a maximum range of 0.8-1.0 amine:epoxide ratio which is within the range indicated by the Instron microbond results. This indicates a maximum just below the stoichiometric ratio which supports the postulate that the presence of amine groups in the sizing can affect the amine:epoxide ratio at the interface and hereby the IFSS. This makes it

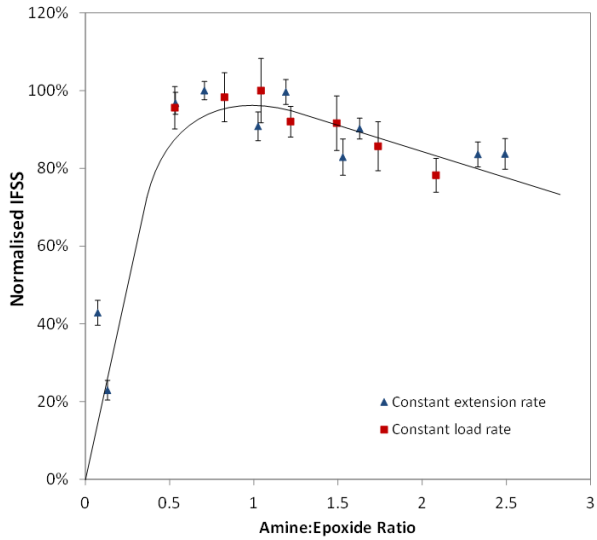

Figure 5.13: Normalised IFSS against the amine:epoxide ratio measured at room temperature with constant extension rate by the Instron (blue) and constant load rate by the TMA microbond setup (red).

possible that increasing the concentration of amine or epoxide groups in the sizing and hereby at the interface could shift the ratio away from the maximum at the stoichiometric ratio.

The testing temperature is mainly of interest when investigating the IFSS or comparing different methods as the maximum IFSS was similar for both the series tested below the glass transition temperature. If a fibre reinforced composite element is used at high temperatures the TMA microbond setup could be a way of discovering the optimal material.

The main difference between the microbond testing using the Instron and the TMA microbond setup is the loading of the samples. The Instron setup uses constant strain rate and the TMA setup constant load rate. This might be the source of the difference in the IFSS values obtained.

6

The influence from sizing on mechanical properties

In this chapter the influence of sizing on the mechanical properties of fibres and composites is investigated, specifically glass fibres with and without sizing are subjected to tensile testing, and laminates manufactured from glass fibres with and without sizing are evaluated by double cantilever beam testing. The first section is based on results published in Paper IV, with the addition of an analysis of fibres modified with GPTMS. The second section contains a procedure and results have not yet been drafted into a manuscript for publication.

6.1 The influence of sizing on the stiffness and strength of single fibres

In section 4.1 it was observed that the fibres after removal of sizing by either soxhlet extraction or burning changed their physical appearance. In this section the mechanical properties of stiffness and strength were therefore investigated of these fibres with pristine fibres as a reference. Furthermore, a batch of fibres have been modified with GPTMS in order to observe changes in the mechanical properties and to obtain the stiffness to be used in a later experiment in section 6.2. GPTMS was chosen as previous studies have shown an enhanced adhesion between glass fibre and epoxy matrix [21, 52, 53]. The stiffness and strength were determined using a single fibre tensile tester, that uses linear density for the determination of the cross sectional area. The pristine fibres were also analysed using the Instron tensile tester used in section 5.1 for comparison of the methods.

The single fibre tensile tester used in this experiment also determined the linear density as a way of calculating the cross sectional area which is needed for the determination of the stiffness of single glass fibres, see eq. 6.1. From eq. 6.2 it can be seen that the density of the fibres is also needed for the calculation of the cross sectional area. The density of the analysed fibres will therefore be determined as a part of the experiment. The linear density is calculated with eq. 6.3 by vibration of the fibres [54]. The linear density is determined of each fibre before testing:

$$E_{fibre} = \frac{F \cdot L_g}{A \cdot \Delta L}, \tag{6.1}$$

where E_{fibre} is the stiffness of the fibres, F is the tension applied during the tensile test, and ΔL is the elongation of the fibre as a result of the tension.

$$A = \frac{\mu}{\rho_{fibre}}, \tag{6.2}$$

where A is the cross sectional area and ρ_{fibre} is the density of the fibres.

$$\mu = \frac{T}{4 \cdot {L_g}^2 \cdot f^2} \tag{6.3}$$

where μ is the linear density, T is the tension at which the measurement was done, L_g is the gauge length of the fibre, and f is the frequency.

6.1.1 Methods

Two types of fibres were analysed: Fibre A and Fibre B. The fibres were divided into three batches. The first batch being pristine fibres were analysed as a reference. A second batch had the sizing removed by soxhlet extraction and a third batch by burning as described in section 4.1 and in Paper I. A fourth batch was made only from Fibre A. They were modified with GPTMS after having the original sizing removed by soxhlet extraction. The fibres were tested using a Single fibre tensile tester, see fig. 6.1. The pristine Fibre A and Fibre B were also tested using an Instron tensile tester.

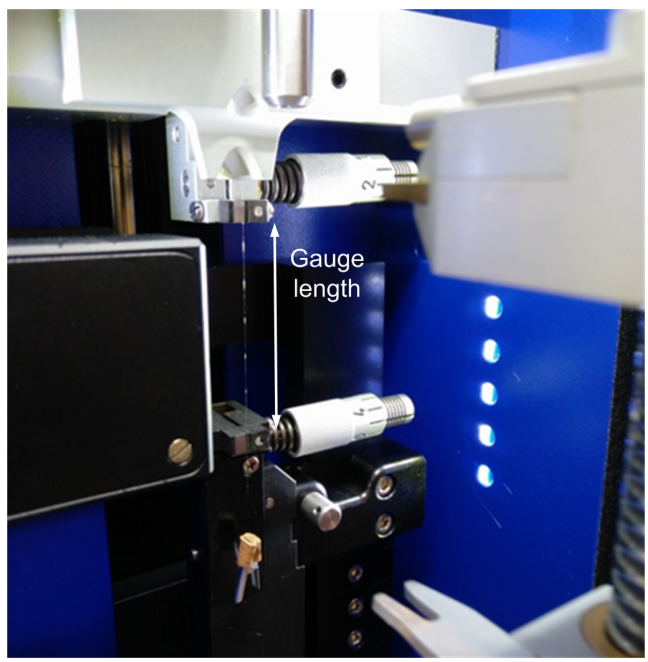

Figure 6.1: The determination of linear density, stiffness and strength using the single fibre tensile tester. The single fibre is clamped yielding a gauge length of 40 mm where it is exposed to acoustic waves followed by extension of the fibre until failure.

Modification with GPTMS

The modification was based on similar approaches from literature [24, 55–60]. The modification was done using fabric UD650 (Fibre A) as they were to be used in a later experiment in section 6.2. The organosilane GPTMS was used for the modification of UD650 fabric. A solution of 1 w/w% GPTMS relative to the fibre weight in deionised water added a few droplets of acetic acid (99.9%) to obtain a pH of 3.5 was mixed at room temperature in a beaker with stirring for 5-10 minutes. The solution was then poured on fibre mats in a container fitting the unrolled sheets and left submersed for 1 hour. The sheets were rinsed with deionised water and subsequently placed in an oven first at 60 °C for 24 hours then for two hours at 120 °C and then left to cool down in the oven.

Density measurement

The measurement was done by using a gas pycnometer with nitrogen as displacement medium. The fibres were dried at room temperature over night in a vacuum chamber before being analysed. The fibres were cut to a length of 5-10 mm to fit in the sample holder. Samples of 2-5 grams were placed in the pycnometer and analysed. Each measurement was repeated a minimum of eight times and the measurement was discarded if the relative standard deviation exceeded a limit of 0.02 % within three consecutive measurements.

Linear density measurement

The linear density was determined prior to each test by measuring the oscillation of fibre vibration induced by acoustic waves, according to ASTM D1577. The diameter of the individual fibre and thus the cross sectional area was calculated using the linear density and the density of the fibres, see eq. 6.2. The measurement was done by the Single Fibre Tensile Tester as a part of the tensile test.

Tensile testing

The determination of the stiffness and strength of single glass fibres was done by tensile test performed on a Single Fibre Tensile Tester. A minimum of 75 individual fibres of each batch of Fibre A and Fibre B (pristine, extracted, burned and modified) were tested with same gauge length of 40 mm and test speed of 1 mm/min. The stiffness was determined from the initial slope in the strain range of 0.05-0.25%. The maximum force measured was used to calculate the strength.

The pristine Fibre A and Fibre B were also tested using the Instron setup by a similar method as presented in section 5.1.1. The samples were made from the same frames as used for the microbond test, but one frame was equal to one sample. The sample frame was cut in the sides leaving the fibre to connect the top and bottom part. The hook in the Instron setup held the sample through the hole that was punched through the top part of the frame. Instead of the microbond fixture a set of clamps were placed in the Instron to fixate the bottom of the frame. The gauge length was 20 mm and the test speed 0.1 mm/min.

6.1.2 FTIR analysis

The modified fibres had the original sizing removed by soxhelt extraction, before being modified with GPTMS. The fibres were weighted before and after the modification, but as fibres

were lost during transfer from the container to the oven the mass loss could not be used as a measure of how much GPTMS had been bonded to the surface. Infrared analysis was conducted on an ATR-FTIR as described in section 4.1 to confirm the presence of GPTMS on the glass fibres. The spectra of the GPTMS modified fibres and the pure GPTMS can be found in fig. 6.2 along with spectra of the pristine Fibre A and the Fibre A after extraction.

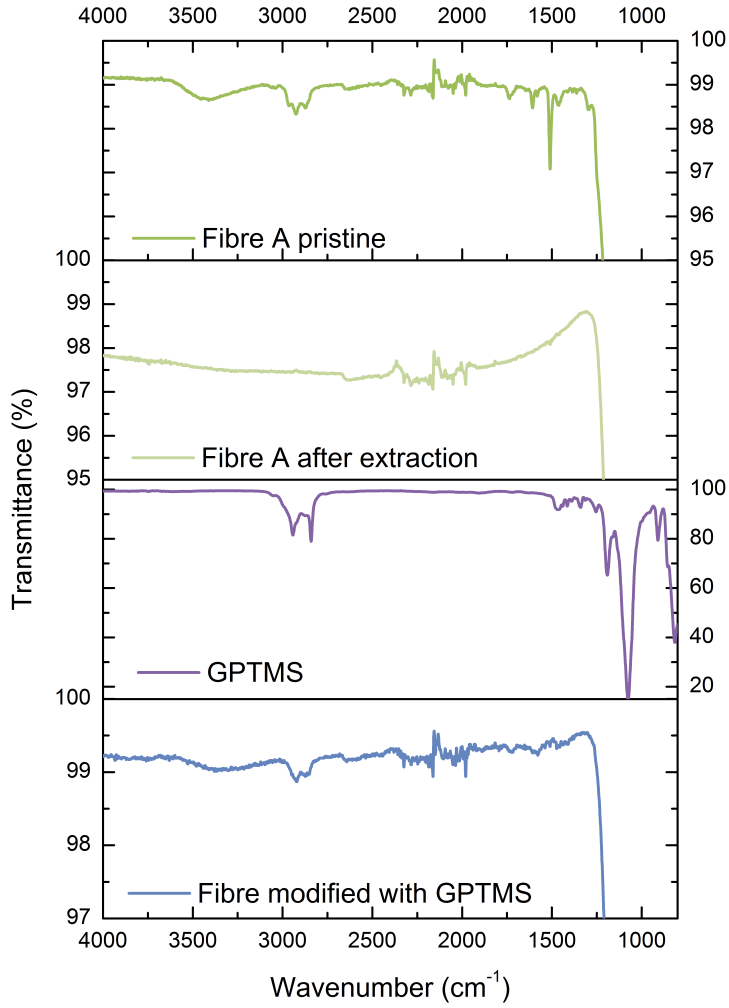

Figure 6.2: FTIR spectra of Pristine Fibre A (green), Fibre A after extraction (light green), pure GPTMS (purple), and GPTMS modified Fibre A (blue).

The pristine fibres and the fibres after extraction exhibit the same bands as identified in section 4.1.3. This applies to both Fibre A and Fibre B. The modified fibres display the Si-O (800-1200 cm^{-1}) and O-H (3200-3600 cm^{-1}) bands related to the glass but also bands from C-H at 2873-2965 cm^{-1}. The signal strength obtained from the analysis of the modified fibres

was very low indicating that the amount of GPTMS is almost undetectable due to the high noise level. The detection of these bands that are not present in the spectrum of the fibres after extraction supports a successful modification.

6.1.3 Density and diameter

The density was determined for Fibre A and Fibre B both as pristine fibres and after soxhlet extraction and burning at 565°C. It was not possible to measure a density of the modified fibres due to lack of material. The density was therefore assumed to be equal to the extracted fibres as the amount of GPTMS bonded to the fibre was negligible in regards to the density. The densities are displayed in 6.3.

The densities of pristine Fibre A (E-glass) and Fibre B (ECR-glass) were 2.58 and 2.72 g/cm^3, respectively, both similar to values found in literature [18]. Removal of the sizing by either extraction or burning both resulted in an increased density which to some extent can be explained by the sizing as follow. From typical sizing components the density of sizing can be estimated to be 1 g/cm^3. Assuming a fibre diameter of 17 μm and a sizing content of 0.60 wt. % it can be calculated that up to 27 and 42 % of the density increase of Fibre A and Fibre B, respectively, can be explained by the removal of the less dense sizing.

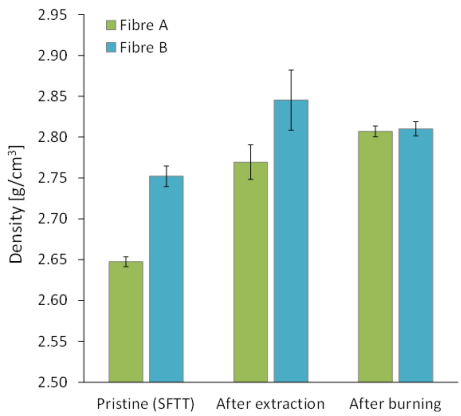

Figure 6.3: Densities of Fibre A (green) and Fibre B (blue) as pristine fibres and after removal of sizing by soxhlet extraction or burning at 565°C.

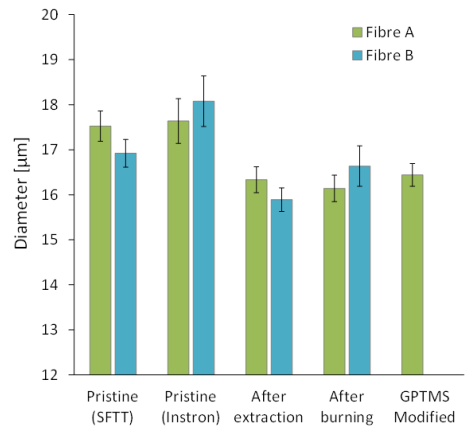

Figure 6.4: Diameter of Fibre A (green) and Fibre B (blue) as pristine fibres, fibres after soxhlet extraction and fibres after burning at 565°C. Additionally the diameter of the GPTMS modified Fibre A is also displayed. The diameter of pristine fibres were determined both as a part of the single fibre tensile test (SFTT) and for the tensile test using the Instron setup.

Fibre A and Fibre B both reach similar densities of around 2.81 g/cm^3 after burning which is very likely as the compositions of the two types of glass are much alike. Both glass types are randomly oriented silicon oxide networks where E-glass (Fibre A) differs by being manufactured with boron oxide and ECR-glass (Fibre B) by containing zirconium oxide instead

[5, 16]. Boron oxide can be a part of the polyhedral network equal to silicon whereas zirconium oxide fits within the tetrahedral structure thus only being able to substitute silicon in tetrahedral parts of the network thus yielding a more stable structure [6]. Burning the fibres at temperatures near the annealing temperature combined with a slow cooling rate could change the bulk structure of the glass fibres towards a more crystalline and stable structure [61] which could make the two fibres structurally more alike. Fibre A display a higher density after burning than after extraction which can be explained by glass compactment of the structure where internal stresses are relaxed. The contraction of the glass yields a higher density [62]. The presence of zirconium oxide in Fibre B provides a structural stability which can explain the higher density of the pristine fibres. The density after extraction and burning are similar and as the structure is already stable it was not expected to be higher after burning.

After extraction the fibres were observed to be very electrostatic as possible antistatic agents in the sizing had been removed, other visible changes were not observed. The burned fibres behaved much stiffer and displayed small kinks from lying on top of other fibres in the roving during heating. This supports that the structure of the burned glass fibres had relaxed to a more rigid network. The extraction is not thought to change the fibres structurally.

The diameters are displayed in fig. 6.4, they were calculated from the cross sectional area derived from eq. 6.2 determined by use of the linear density. The burned fibres were expected to exhibit a decrease in diameter compared to the pristine fibres based on the compactment of the glass. A small decrease was observed, but the fibres after extraction display the same small decrease of diameter which cannot be explained by removal of the less than 100 nm thick sizing. The large scatter in diameter of all the glass fibres obstructs small changes in the fibre diameter caused by alteration of size and shape. The diameter of the GPTMS modified Fibre A is also displayed in fig. 6.4. It was calculated by assuming a density of the fibres equal to Fibre A after extraction and the diameter was similar to these fibres. The fibre diameters of the pristine fibres determined in connection to the Instron setup were obtained by image analysis and seem to be slightly larger compared to those calculated from the linear density.

6.1.4 Stiffness and strength

Even though up to 125 fibres in a batch were tested a large fraction of the data was omitted. Some fibres broke while exposed to acoustic waves as a part of the determination of linear density prior to the tensile test or in the initial part of the tensile test. If two fibres were tested simultaneously by mistake or if the fibre slipped between the clamps during testing these data would also be excluded. The burned fibres were especially troublesome to test since they were extremely fragile. In general 60-73 fibres of each batch were tested without the above mentioned issues whereas less than 50 of the burned fibres were possible to test. The stiffness and strength of Fibre A and Fibre B as pristine fibres, fibres after extraction, burning or modification determined by the use of the single fibre tensile tester are displayed along with the strength and stiffness of Fibre A and Fibre B determined using the Instron tensile tester in fig. 6.5 (stiffness) and fig. 6.6 (strength).

The stiffness of pristine Fibre A and Fibre B were determined to be 77 GPa and 80 GPa, respectively, which were similar to values found in literature [16, 18]. Removal of the sizing by either extraction or burning increased the stiffness by 3-9 GPa. This corresponds to similar studies of heat treated glass fibres from literature that explain it by relaxation of the stresses induced during manufacture by rapid cooling [18, 62].

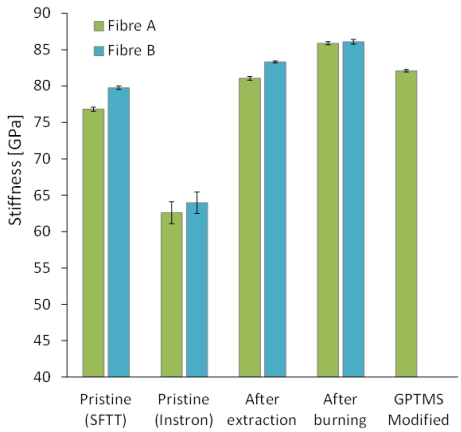

Figure 6.5: The stiffness of Fibre A (green) and Fibre B (blue) as pristine and after removal of sizing by extraction or burning, obtained by single fibre tensile testing. The stiffness of pristine fibres were determined both as a part of the single fibre tensile test (SFTT) and for the tensile test using the Instron setup.

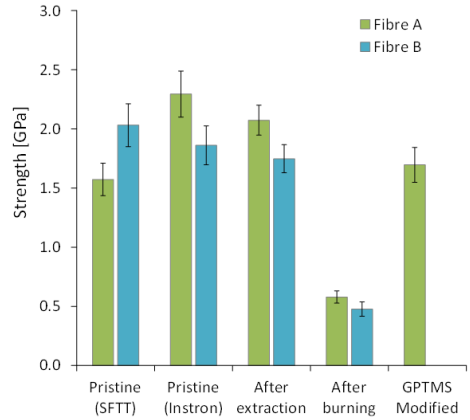

Figure 6.6: The strength of Fibre A (green) and Fibre B (blue) as pristine and after removal of sizing by extraction or burning, obtained by single fibre tensile testing. The strength of pristine fibres were determined both as a part of the single fibre tensile test (SFTT) and for the tensile test using the Instron setup.

The stiffness determined by the Instron were much lower than expected even with the difference in gauge length [63]. Compliance correction is recommended, but was not possible since only one gauge length was used, which could result in the measurede value being too low. The longer the gauge length the lower the compliance factor [63]. An additional explanation could lie in the factor 10 difference in testing speed. However the strength determined by using the Instron setup is similar to the values determined using the single fibre tensile tester with a small difference in the measurement of Fibre A and an even smaller difference in the values of Fibre B.

The pristine fibres exhibit a strength much lower than values found in literature where a strength of around 3 GPa is listed [5, 16, 18]. However the fibres still demonstrate a decrease in strength after burning and to a level as expected from literature [62, 64–66]. This reduction in strength is related to the enlargement of flaws already present on the fibre surface which becomes vulnerable to water attacks [65]. The strength of the fibres after extraction is similar to the pristine fibres with a very small increase for Fibre A and decrease for Fibre B. Despite the strength of the pristine fibres and the fibres after extraction being lower than expected they are close to strength values obtained of bare E-glass fibres with no sizing [66].

The Fibre A modified with GPTMS exhibted stiffness similar to the extracted fibres, but a strength that was closer to the pristine fibres as expected since the fibres have not been exposed to high temperatures during the modification. The extra handling steps by modifying the fibres could cause damage to the fibres that were more vulnerable to water attacks while being without sizing yielding a lower strength.

6.1.5 Summary

Removal of the sizing by soxhlet extraction or by burning at 565°C increased the density of Fibre A by 5% and 6%, respectively. Similar for Fibre B where extraction and burning lead to an increase of 3% and 1%, respectively. The increase in density was to some extent explained by the removal of the less dense sizing and for the burned fibres also the compactment of the glass structure.

The stiffness of Fibre A increased from 77 GPa to 81 GPa after removal of sizing by extraction and 86 GPa after burning. In contrast the strength of Fibre A was found to decrease after burning from 1.6 GPa to 0.6 GPa whereas the fibres after extraction increased in strength to 2.1 GPa. Similar results were observed for Fibre B in that the stiffness increased from 80 GPa to 83 GPa after extraction and 86 GPa after burning. The strength of Fibre B also displayed a large decrease after burning from 2.0 GPa to 0.5 GPa where the extraction led to a less significant decrease to 1.8 GPa. The behaviour of the burned fibres were explained by relaxation of the glass structure and enlargement of flaws yielding an increase in stiffness and a decrease in strength, respectively. The cause of the increase in strength after removal of the sizing by extraction has not been uncovered, but could be related to the healing effect of sizing in regard to surface flaws [67–69].

The GPTMS modified Fibre A displayed stiffness and strength values as expected from the handling. The two glass fibre types, E- glass and ECR-glass, did not exhibit characteristics that can distinguish one from the other. Using the two different methods, single fibre tensile tester and the Instron setup displayed a clear discrepancy in the determined stiffness of the pristine Fibre A and Fibre B which was less evident in the diameter and strength determinations. This clearly emphasises the importance of using these methods with caution when comparing with studies using other methods and equipment.

6.2 The influence of sizing on interface adhesion

When moving from investigating a single fibre embedded in a droplet to bundles of fibres in fibre reinforced polymer composites, it is no longer possible to study the individual fibres and their load. The fibre debonding can however be displayed in a different manner, by fibre bridging during double cantilever beam testing (DCB) in which the strength of bonding can be determined. The determination of the energy of the bonded surfaces is done in this experiment as a measure of the adhesion between fibre and matrix. It is repeated that, fibres with a strong adhesion to the matrix would rather breake, than being pulled out during crack propagation [14]. The effect of the glass fibre sizing on the adhesion between glass fibres and polymer matrix, was investigated using DCB specimens by determination of the J-integral. Three individual laminates manufactured from fabric were investigated by DCB testing with small scale specimens: one laminate where the fibres had their original sizing, a second where the sizing had been removed by extraction and a third laminate where a new coating in the form of GPTMS had been applied. In addition to the J-integral analysis the manufacturing of the laminates and the DCB specimens is thoroughly covered in this section.

DCB testing is an often used experimental method within fracture mechanics. Fractures observed in DCB specimens can be divided into three modes depending on the orientation of the force applied leading to crack propagation, see fig. 6.7. Mode I fracture occurs when a tensile load perpendicular to the crack plane is applied to the beams. Mode II fracture is in-plane shearing caused by shear forces applied parallel to the crack plane and parallel to the

crack direction. Mode III fracture is out-of-plane shearing in which the shear force is applied parallel to the crack plane but perpendicular to the crack direction.

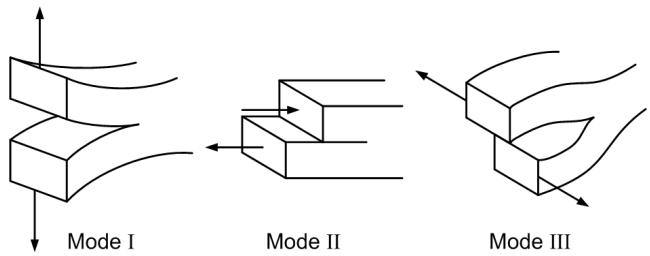

Figure 6.7: The three fracture modes. Mode I is the opening mode. Mode II is the in-plane shear. Mode III is the out-of-plane shear.

The testing rig used in this experiment provides a mode I fracture where the crack propagates along the fibre direction. This yields a simpler calculation of the fracture surface energy as shearing forces are avoided. When a crack propagates thus forming new surfaces, energy is released from the strained area around the crack tip. The energy needed for a crack to propagate is denoted as G_C. The bridging behind the crack tip results in a large scale fracture process zone denoted as the bridging zone. Since the material is non-linear elastic and with bridging, the energy cannot be calculated through the strain energy release rate (G) from the fracture toughness (K_{IC}). The J-integral can however still be determined, but not from the strain energy release rate as it only applies to linear elastic materials at which it is equal to the J-integral [70].

The J-integral can be calculated by using the cohesive law that applies in the bridging zone as the J-integral is the work per fracture area by bridging stress, see eq. 6.4:

$$J = \int_0^{\delta^*} \sigma_b(\delta) d\delta, \tag{6.4}$$

where σ_b is the bridging stress and δ^* is the displacement at the bridging zone.

Conversely it is possible to obtain the bridging law from the J-integral and the bridging zone opening by differentiation as in eq. 6.5:

$$\sigma_b(\delta^*) = \frac{\partial J}{\partial \delta^*} \tag{6.5}$$

The J-integral is path independent making it possible to calculate the stresses at the crack tip from paths located away from the crack tip for more convenient calculations [71]. The J-integral is often calculated from the crack length [72], which can be difficult to obtain in the laboratory. The used DCB testing rig applies pure moment bending. As a result, the J-integral becomes independent of the crack length simplifying the calculation to eq. 6.6 [23]:

$$J = (1 - \nu^2) \cdot \frac{12 \cdot M^2}{B^2 \cdot H^3 \cdot E_{11}}, \tag{6.6}$$

where ν is poisson's ratio, M is the moment, B is the hight of the specimen, H is the width of one beam and E_{11} is the longitudinal stiffness. The dimensions are illustrated later fig. 6.12.

Furthermore, usage of mode I fracture entails that the out-of-plane stress (σ_{33}) equals zero further simplifying the expression. In order to calculate the J-integral from eq. 6.6 the longitudinal stiffness is needed which can be obtained by the rule of mixture [4] in eq. 6.7:

$$E_{11} = (1 - V_{fibre}) \cdot E_{matrix} + V_{fibre} \cdot E_{fibre}, \tag{6.7}$$

where V_{fibre} is the fibre volume fraction, E_{matrix} and E_{fibre} are the stiffness of matrix and fibre, respectively.

The strength and stiffness of the fibres were investigated in section 6.1 and the volume fractions of fibre and matrix are determined as a part of the characterisation of the laminates manufactured for the DCB specimens in this section.

6.2.1 Methods

Three laminates were manufactured by vacuum infusion of unidirectional (UD) non-crimp glass fibre fabric and Epoxy matrix 2. The fabric UD650 (made from Fibre A) was the target of the investigation. A second fabric UD950 was used merely as filling in the laminate.

The three laminates were manufactured from fabrics with the original sizing (REF), without sizing (EXT) and with a new sizing (MOD). The sizing was removed using soxhlet extraction as in section 4.1. The modification was conducted with GPTMS as described in section 6.1.1.

The sheets of both UD650 and UD950 were cut in the dimensions of 100 mm$\times$250 mm with the fibre direction along the short side. Prior to the treatment and layup for the infusion the stitching of the UD650 fabric was removed leaving only three rows of stitching in the top and bottom part, see fig. 6.8. The removal of sizing from the two batches of UD650 was done in a large soxhlet. The sheets were loosely rolled before being placed in the 250 mL soxhlet, see fig. 4.2.

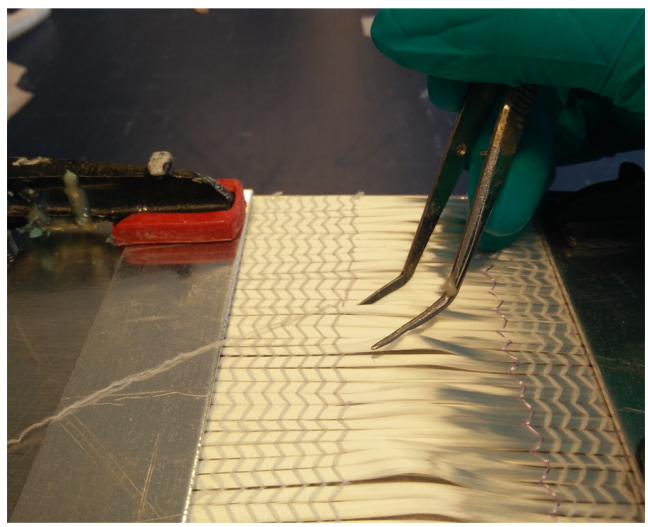

Figure 6.8: The stitching keeping the rovings in the fabric is removed manually. The sheet of fabric is fixated by press plates to minimise disorder among the rovings.

Laminates

The layup of the laminate is illustrated in fig. 6.9 and fig. 6.10 with eight sheets of UD950, then two sheets of UD650 and finally eight sheets of UD950 again. The UD950 were placed with the backing away from the middle. A 12.5 μm thick slipfoil (30 mm$\times$250 mm) was placed between the two UD650 sheets. A peelply was placed underneath and on top of the glass fibre sheets and with a press plate on top of the layup. The matrix inlet was placed along the same side as the slipfoil and the outlet for the vacuum pump was on the other side. The matrix was mixed in the weight ratio of 100:28 of epoxy resin and curing agent, respectively, and subsequently degassed. The layup was arranged on a glass plate with a slip coat and then sealed with a vacuum bag. The infusion was done at 85% vacuum which was reduced to 60% as soon as the resin had left the fibres. The peelply was twice the length of the fibres to function as a brake of the matrix. When the resin had reached the outlet tube the vacuum bag was closed. A heating blanket was used for the first part of the curing: 19 hours at 40 °C, then subsequently 5 hours at 75 °C.

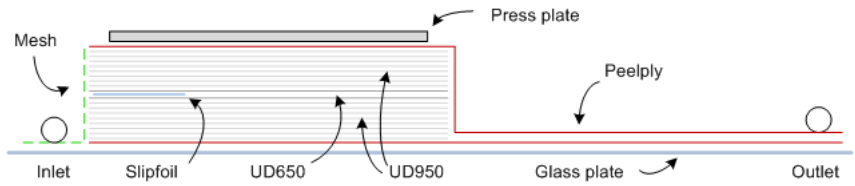

Figure 6.9: Cross section of the layup of the laminate as seen from the side. Not to scale.

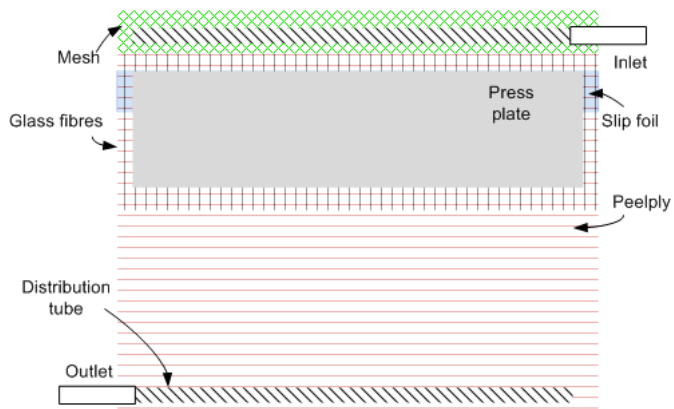

Figure 6.10: Layup of the laminate as seen from above. Not to scale.

Volume fraction determination

Samples for the volume fraction determination was cut from the part of the laminate just below the slipfoil. Two samples were cut from each of three slices of the laminate yielding six cubes of approximately 10 mm$\times$10 mm$\times$10 mm. Edges were polished to avoid cutting residue that could trap bubbles during weighing in water. The samples were then dried for a minimum of 16 hours at 0.7 bar and afterwards kept in a desiccator while cooling down.

The samples were weighted in air and in boiled deionised water using an Archimedes setup, fig. 6.11, in order to obtain the density of the composite. Prior to the weighing in water the samples were sealed using a 20 wt.% paraffin in petroleum ether. The density of the composite was calculated using eq. 6.8:

$$\rho_{composite} = \frac{m_{sample,a} \cdot \rho_{water}}{m_{sample,s} - m_{sample,w} - \frac{\rho_{water} \cdot (m_{sample,s} - m_{sample,a})}{\rho sealing}}, \tag{6.8}$$

where $\rho_{composite}$, ρ_{water}, and $\rho_{sealing}$ is the density of the composite, the water, and the sealing, respectively. m_{sample} is the mass of the sample in air, sealed and in water, denoted a, s and w, respectively. The density of water was calculated as a function of the water temperature [73].

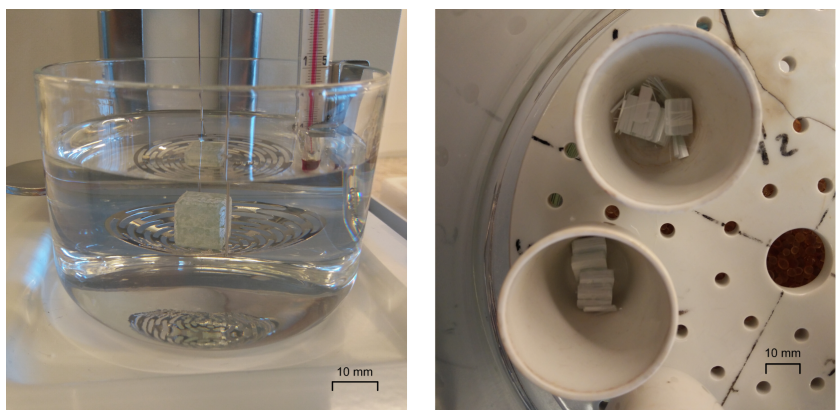

Figure 6.11: The left image displays a sealed sample being weighed in water with the Archimedes setup. The image on the right displays the samples in crucibles after burning cooling down in a desiccator.

After weighing in water the samples were burned at 450 °C for 2-4 hours in annealed crucibles. The samples were weighed before and after burning, fig. 6.11, in order to obtain the weight fractions, see eq. 6.9 and 6.10:

$$W_{fibre} = \frac{m_{fibre}}{m_{sample,a}} \cdot 100\%, \tag{6.9}$$

$$W_{matrix} = 100\% - W_{fibre}, \tag{6.10}$$

where W_{fibre} and W_{matrix} are the weight fractions of fibre and matrix. m_{fibre} is the mass of fibre left after burning of the sample and $m_{sample,a}$ is the mass of the sample before sealing.

The volume fractions of fibre, matrix, and porosity, noted V_{fibre}, V_{matrix} and $V_{porosity}$, were calculated using eq. 6.11, 6.12, and 6.13:

$$V_{fibre} = \frac{\rho_{comp} \cdot W_{fibre}}{\rho_{fibre}} \tag{6.11}$$

$$V_{matrix} = \frac{\rho_{comp} \cdot W_{matrix}}{\rho_{matrix}} \tag{6.12}$$

$$V_{porosity} = 100\% - V_{matrix} - V_{fibre} \tag{6.13}$$

DCB specimens

Specimens were cut within the area of the press plate to ensure the dimensions. The length of the specimens were 70 mm with 20 mm being with slipfoil. The specimens were cut to be <4.9 mm wide to fit the DCB testing rig. A schematic illustration of the specimens can be found in fig. 6.12. The samples were polished with grain 500 (2×15 sec.) and 1200 (2×10 sec.). The notch for the fixture was made with a milling cutter. Black painted tape was placed to mark the edges, on each edges of tape a mark was made to be used for the crack opening displacement determination. Seven specimens of each laminate, were tested using the DCB testing rig.

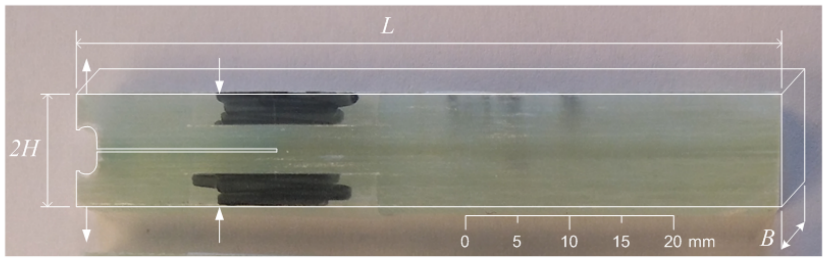

Figure 6.12: Drawing and image of the DCB specimens.

Testing

The testing rig is a custom made fixture described by Sørensen et al. [74]. The DCB specimens were tested with pure moment loading by constant displacement speed. The loading occurs when the two parts of the rig are moved apart straining the band around the rollers and hereby opening the DCB specimens. The testing rig loading a DCB specimen is illustrated in fig. 6.13. The initial crack tip determined by the slip foil placed after the point of pressure. The load and thereby the moment was recorded by a DasyLab program simultaneously with a video of the crack tip zone obtained with a microscope through the DeltaPix program throughout the whole testing. The DCB testing rig is fixated to a xyz board and moved during testing to keep the initial crack tip within the field of view.

The determination of the crack tip opening, was done manually through images obtained from the video by digitally measuring between the two marks identifying the position of the initial crack tip using the program ImageJ. Images obtained from a testing video are displayed in fig. 6.14, one image from before loading and a second just before failure of the specimen. An image of the crack tip zone was taken just before starting the test, in order to obtain a zero value of the distance between the two marks in the crack tip zone. The distance in pixels was converted to millimetres by measuring the scale bar set by DeltaPix, which had been calibrated to an external scale bar. The video was shot with one frame per second and yielding an image size of 1616 pixel×1216 pixel equal to 7.48 mm×5.63 mm. A linear variable differential transformer (LVDT) was used to monitor the opening of the specimen during the DCB test. This opening is not used for the calculations of the J-integral.

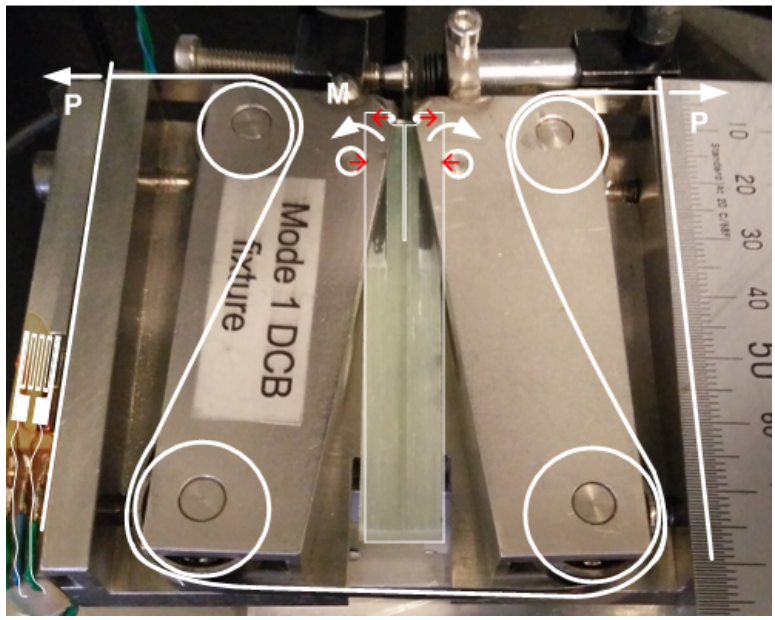

Figure 6.13: Combined drawing and image of the DCB testing rig showing the position of the specimen and the spools responsible of the pure moment loading.

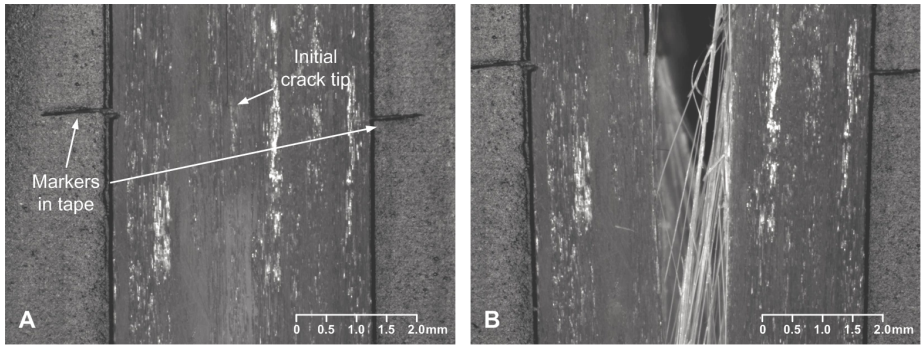

Figure 6.14: Images of a DCB specimen obtained from the video recorded during testing displaying the initial crack tip zone at the beginning (A) and at the end of the test (B).

6.2.2 Prerequisites for calculating the J-integral

The parameters determined and calculated in order to be able to quantify the J-integral, are listed in tab. 6.1 for all three laminates. The density and stiffness of the used fibres were determined in section 6.1. The density of the composite was determined as described using Archimedes law. Weight and volume fractions of fibre, matrix and porosity were calculated as a part of the volume fraction determination. The equations can be found in section 6.2.1. The longitudinal stiffness was calculated using the rule of mixture, from the volume fraction of fibre in the laminate and the stiffness of the single fibres, see eq. 6.7.

Table 6.1: Table containing the parameters used for the calculation of the J-integral. The density and the stiffness were determined in section 6.1. The density of the composite and the weight and volume fractions of fibre, matrix and porosity were calculated as a part of the volume fraction determination. The longitudinal stiffness was calculated using the rule of mixture.

	REF	EXT	MOD
ρ_{fibre} (g/cm^3)	2.65	2.77	-
E_{fibre} (GPa)	76.8	81.1	82.1
$\rho_{composite}$ (g/cm^3)	1.96	1.92	2.00
W_{fibre} (%)	74	72	76
W_{matrix} (%)	26	28	24
V_{fibre} (%)	55	53	57
V_{matrix} (%)	44	45	41
$V_{porosity}$ (%)	2	2	2
E_{11} (GPa)	43.5	44.1	48.3

The density of the MOD composite is slightly higher than both the REF and the EXT laminate, but the volume fraction is also equivalently higher. The stiffness of EXT and MOD fibres were similar partly because they both were calculated based on the density of the EXT fibres. Combining the high stiffness and the higher volume fraction of fibres yield a higher longitudinal stiffness. The fibre volume fraction, the density of the composite and the void content were found to be close to those obtained for similar laminates in literature [75].

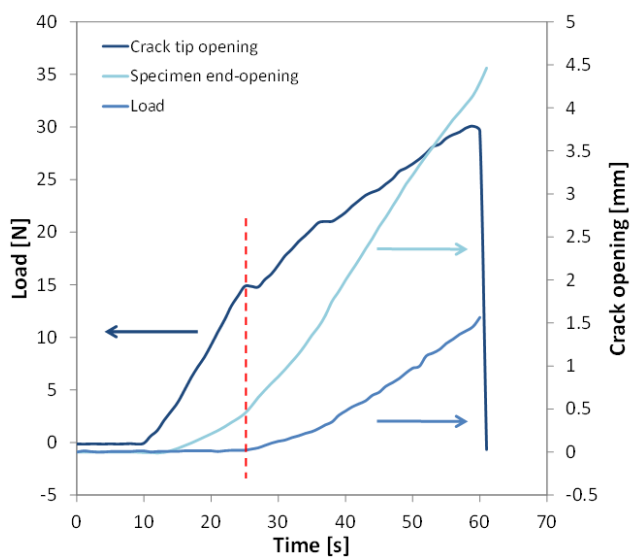

Figure 6.15: The load (dark blue) the crack tip displacement (blue) and the specimen end-opening (light blue) measured as a function of the duration of the DCB testing. The red line marks the separation of the two stages of the specimen opening.

The applied load was measured continuously and the corresponding crack tip opening displacement (δ^*) was determined from the video recorded during the DCB test. Both are displayed against time in fig. 6.15 along with the end-opening of the specimen. The displacement initiated long after the loading has begun. This is also true for the crack tip opening, but the end-opening displacement (δ) of the specimen begins along with the loading. The loading curve has two stages; the initial loading where only the end of the specimen is opening until a certain point marked with a red line in fig. 6.15. After this point the second stage of the loading take place with increase in the crack tip opening until failure point. The slope of the loading and the specimen end-opening change as the displacement at the crack tip initiate. The reason for the delay in displacement at the crack tip, is the deformation in the beams in the initial stage of the DCB test [76]. As the beam deformation becomes almost constant, bridging will start as the crack propagates along the specimen. This is one of the main reasons why the crack tip opening is measured and used for the calculation of the J-integral instead of the specimen opening.

6.2.3 The J-integral

The J-integral was calculated as in eq. 6.6. The results of the DCB testing of the three laminates are displayed in fig. 6.16, 6.17, and 6.18. Additionally a collection of all the J-integral curves is displayed in fig. 6.19 for comparison.

During the testing unevenness in the crack propagation can occur and with small load drops as result. The crack do not grow until the previous level of load is reached again. An iterative analysis was conducted in order to even out the curves by removing these load drops. A maximum decrease in the J-integral was set from a tolerance parameter of approximately 5 ‰of the maximum value of the J-integral [77]. Decreases above this limited were disregarded.

The J-integral curves obtained from testing the REF laminate were all coinciding having a J_0 values of approximately 100 J/m^2 and similar slopes. J_0 is the surface energy at the crack tip and can be compared to the energy needed to initiate the exposure of new surface area by crack growth causing bridging. The slope indicates how much energy is needed for the crack to propagate. Both parameters are related to the strength of the adhesion between fibre and matrix. It is expected that a strong interface will result in a high J_0 and a steep slope as more energy is needed for the bridged fibres to either break or debond along the fibre surface. The progress of the J-integral does not appear to reach a steady state level as expected before failure of the specimen. At the steady state level the length of the bridging zone becomes constant following the crack tip. The length of the DCB specimens is the reason for the lack of a steady state level of the J-integral as the length of the bridging zone exceeds the length available.

The EXT laminate yielded similar curves but with a J_0 a little above 100 J/m^2 and a slope similar to the results of REF. However one specimen resulted in a J-integral curve behaves a little differently from the rest. It has a lower J_0 and in fig. 6.19 it is located together with the results obtained for the REF specimens instead. This behaviour can be explained by an uneven removal of the original sizing. During the extraction process the fabric is rolled before being placed in the soxhlet which might create a void where the washing of the fibres is less effective. This means that the fibres bridging in this specimen could still have a little of the original sizing on the surface. Generally it can be seen that the EXT curves lie above the REF curves and the EXT specimens reach a higher crack tip opening before failure. This indicates

that the removal of the original sizing on Fibre A has resulted in a slightly stronger interface between the glass fibre and the epoxy matrix.

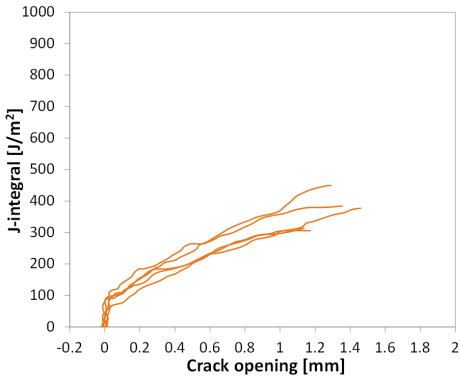

Figure 6.16: J-integral curves for the DCB testing of specimens from the reference laminate (REF).

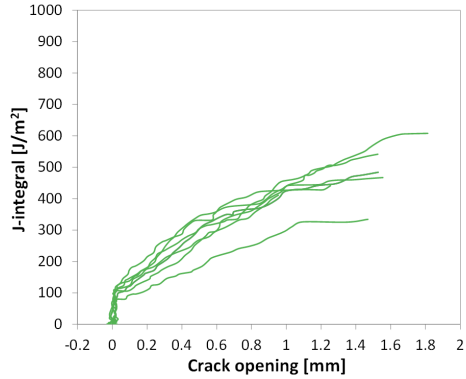

Figure 6.17: J-integral curves for the DCB testing of specimens from the laminate manufactured from fibres with the sizing removed (EXT).

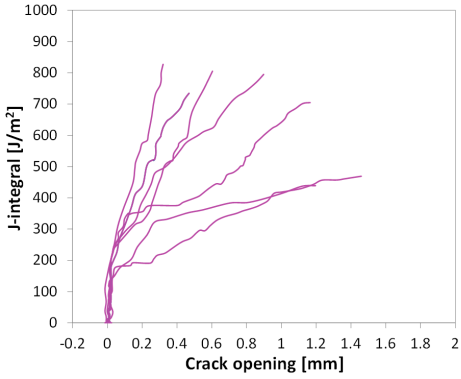

Figure 6.18: J-integral curves for the DCB testing of specimens from the laminate manufactured from fibres modified with a GPTMS coating (MOD).

Where both the REF and the EXT yields J-integral curves, that coincide well the opposite applies for the MOD results that has a large scatter like a bouquet of flowers. Two curves specifically differ from the rest by a J_0 around 150 J/m^2 and a less steep slope, whereas the others display a J_0 above 200 J/m^2 and a wide span of steep slopes. Only one of the specimens failed before the maximum loading was reached. The corresponding curve is the one with the lowest J_0 and slope. The maximum load is a limitation in the displacement of the two parts of the testing rig. When examining the specimens under microscope after testing a clear tendency was uncovered as the two specimens with J_0 around 150 J/m^2 exhibited the

one crack that would be expected. The rest displayed evidence of two or more cracks. This behaviour has also been found in literature [78]. As the fracture surface area increases with an additional crack the steady state level is also increased. More energy is needed to initiate the opening at the crack tip and for the crack to propagate through the DCB specimen. This indicate that by applying a new coating of GPTMS it was possible to enhance the adhesion between fibre and matrix.

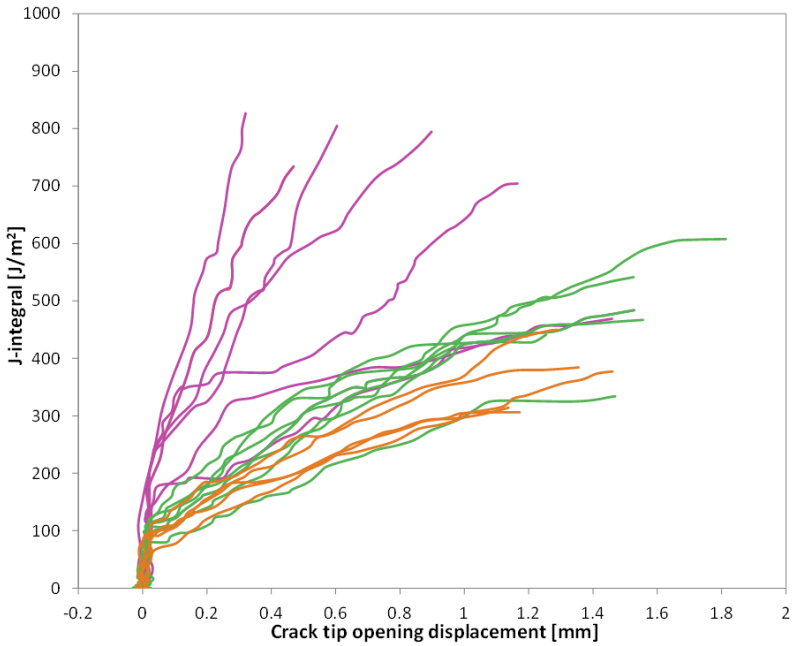

Figure 6.19: All the J-integral curves together comparing the adhesion in the three laminates REF (orange), EXT (green) and MOD (pink).

6.2.4 Summary

The aim of the DCB testing was to see if changing the sizing of glass fibres could affect the strength of the interface adhesion and if it was possible to be determined by the measure of the J-integral. The laminates investigated were comparable to laminates in literature in regard to physical properties [75].

It was indeed possible to use the DCB testing of small scale specimens to investigate how changes in the chemistry of the interface affected the adhesion between glass fibres and matrix.

Removal of the sizing by soxhlet extraction yielded a slightly stronger adhesion between fibre and matrix compared to the reference material with the original sizing. The extractable components must not contribute positively to the adhesion at all. By removing the extractable part of the original sizing and applying a GPTMS coating on the fibres is was possible to obtain a clear difference. Both the energy needed for initiating the crack tip opening, and the energy for the crack to propagate causing bridging of the fibres were remarkably higher than

the obtained values for the reference laminate and the laminate from fibres without sizing. It was found possible to develop a coating for the glass fibres yielding a significant higher interface adhesion than with the original sizing.

The examination of the results obtained from the DCB testing focus on the determination of the J-integral. More information about the fibre bridging can be derived from the J-integral and the fibre bridging stress is obvious as the next step.

7

Conclusions and perspectives

The investigation of the sizing on the glass surfaces yielded the following conclusions:

It was possible to burn off more sizing at 565 °C, than was extractable by soxhlet extraction using acetone, indicating that a residue of the organic part of the sizing was left at the surface and that organic components were directly or indirectly bonded to the glass fibre surface. The sizing might be unevenly distributed as a large variation in the extractable amount of sizing was observed. Characterisation of two commercial glass fibres indicated that distinguishing between them is difficult. However, a DGEBA derivate was identified as the film former in both sizings through ATR-FTIR and TGA-MS analysis, thus epoxide groups are present. Indications of a lubricant/surfactant in the form of polyethylene oxide were also detected. Functional groups from the silane coupling agent were not identified. Glass plates were dip-coated with organosilanes as a way of mimicking the glass fibre surface. The deposition of organosilane was confirmed by ATR-FTIR. The results also indicated that the organosilane was bonded to the surface. The glass surface was more polar after the dip-coating, implying that the presence of an organosilane significantly changes the surface properties.

The investigation of the IFSS measured by microbond testing leads to the following conclusions:

Varying the ratio between amine and epoxide groups of the epoxy affected the debonding of droplets on single glass fibres. A maximum IFSS was detected around the stoichiometric ratio of the epoxy. It is believed that sizings containing functional groups as amine and epoxide can shift the ratio away from which the maximum IFSS is found. Testing temperature also influenced the IFSS with the highest values determined at room temperature. When the testing temperature exceeds the glass transition temperature, the IFSS behaviour changes, and becomes linear as function of the amine:epoxide ratio. The usage of two different microbond setups yielded results that revealed a certain difference in the measured IFSS. The two setups used constant strain rate and constant load rate, respectively, presumed to be the root of the difference.

The investigation on the influence of sizing on mechanical parameters resulted in the following conclusions:

The stiffness of the single fibres increased after removal of the sizing both by soxhlet extraction and by burning at 565 °C. The increase was partly explained by the removal of the less dense sizing and for the burned fibres also by compactment of the glass structure. The strength of the fibres on the other hand decreased notably after burning due to enlargement of surface flaws. The changes after extraction were less significant, most likely since the non-extractable sizing would retain the healing effect on surface flaws. Fibres that had the original sizing removed by soxhlet extraction and a new coating of GPTMS applied subse-

quently displayed both stiffness and strength values similar to those obtained for the fibres after extraction. The modification was confirmed with ATR-FTIR even though no increase in mass was detected. The amount of GPTMS deposited on the fibres was therefore considered insignificant for the density of the fibres. The DCB testing of small scale specimens proved applicable for the investigation of the influence of sizing on the interface adhesion by the determination of the J-integral. It was possible by a simple coating of GPTMS to achieve a significant higher interface adhesion compared to the original sizing. The rather rough modification yielded a large scatter whereas the results obtained from the fibres with the original sizing exhibited much less dispersion. It was deduced that the GPTMS modification was very uneven compared to the original sizing. The removal of the extractable sizing resulted in slightly improved adhesion. It was therefore concluded that the extractable part of the sizing did not facilitate strong adhesion.

Perspectives

The following is a list of experiments and investigations that could lead to a further understanding of how a strong interface adhesion can be achieved with higher control than obtained in this thesis:

- An extraction investigation in regard to time and solvent. How much sizing can be extracted, and how quickly?
- GC-MS and ToFSIMS analysis on both sizing extract and glass fibres to obtain more knowledge about functional groups present.
- Expand the microbond investigation to include extreme amine:epoxide ratios, lower testing temperatures, different sizings e.g. no sizing/water, GPTMS, also different concentrations of sizing.
- Investigate how quickly the film former can be dissolved in the matrix. Should the film former be removed prior to the manufacture of the composite in order to obtain a stronger adhesion?
- Determination of the density of GPTMS modified fibres to confirm assumption of a density equal to the one for fibres after extraction.
- Gain more control of the modification procedure to obtain an even distribution of the coating.
- A lot more DCB testing on the small scale specimens for the continued investigation of how the surface chemistry (sizing) affects the interface adhesion by comparing fibres with different sizings and by producing more modified fibres. Also investigating different manufacturing methods of the laminate e.g. thinner laminates without filling fabric, filament winded laminates.
- Further investigation of the bridging law and the relations to the single fibre bridging.

Bibliography

[1] G. H. Staab, *Laminar Composites*. Oxford, United Kingdom: Butterworth-Heinemann, 1999.

[2] J. L. Ferracane, "Developing a more complete understanding of stresses produced in dental composites during polymerization," *Dental Materials*, vol. 21, no. 1, pp. 36–42, 2005.

[3] B. Roeseler, W. G. amd Sarh and M. U. Kismarton, "Composite structures: the first 100 years," in *Proceedings of the Sixteenth International Conference on Composite Materials. 8-13 July, Kyoto, Japan*, Japan Society of Composite Materials, 2007.

[4] F. C. Campbell, *Structual composite materials*. Ohio, United States: Materials Park, 2010.

[5] P. Brøndsted, H. Lilholt, , and A. Lystrup, "Composite materials for wind power turbine blades," *Annu. Rev. Mater. Res.*, vol. 35, no. 1, pp. 505–538, 2005.

[6] D. W. Dwight, "Glass fibre reinforcement," in *Comprehensive composite materials* (A. Kelly and C. Zweben, eds.), vol. 1, pp. 231–61, Amsterdam, Netherlands: Elsevier, 2000.

[7] J. L. Thomason, *Glass Fibre Sizings – A Review of the Scientific Literature*. Glasgow, Scotland: University of Strathclyde, 2012.

[8] H. G. Willett, "Characterisation of composites for wind turbine blades," *Reinforced Plastics*, vol. 56, no. 5, pp. 34–36, 2012.

[9] R. L. Gorowara, W. E. Kosik, S. H. McKnight, and R. L. McCullough, "Molecular characterization of glass fiber surface coatings for thermosetting polymer matrix/glass fiber composites," *Compos. Part A: Appl Sci Manuf*, vol. 32, no. 3-4, pp. 323–329, 2001.

[10] J. L. Thomason, "The interface region in glass fibre.reinforced epoxy resin composites: 3. characterization of fibre surface coatings and the interphase," *Compos.*, vol. 26, no. 7, pp. 487–498, 1995.

[11] J. G. Taylor, "Chapter 12: Composites," in *Phenolic Resins: A Century of Progress* (L. Pilato, ed.), pp. 267–269, Berlin, Germany: Springer, 2010.

[12] R. McMican, "Sizing stability is a key element for glass fibre manufacturing," *Reinforced Plastics*, vol. 56, no. 5, pp. 29–32, 2012.

[13] B. F. Sørensen, J. W. Holmes, P. Brøndsted, and K. Branner, "Blade materials, testing methods and structural design," in *Wind Power Generation and Wind Turbine Design* (W. Tong, ed.), pp. 417–465, Ashurst, United Kingdom: WIT Press, 2010.

[14] S. Feih, K. Wonsyld, D. Minzari, P. Westermann, and H. Lilholt, "Testing procedure for the single fibre fragmentation test," tech. rep., Risø National Laboratory, 2004.

[15] M. Dey, J. M. Deitzel, J. W. Gillespie Jr., and S. Schweiger, "Influence of sizing formulations on glass/epoxy interphase properties," *Compos. Part A: Appl Sci Manuf*, vol. 63, pp. 59–67, 2014.

[16] F. R. Jones, "Glass fibres," in *High-performance fibres* (J. W. S. Hearle, ed.), pp. 191–238, Cambridge, England: Woodhead Publishing Ltd., 2001.

[17] M. P. Stevens, *Polymer Chemistry an Introduction*. Oxford, United Kingdom: Oxford University Press Inc, 1999.

[18] D. Hartman, M. Greenwood, and D. Miller, "High strength glass fibers," tech. rep., Owens Corning Corp., 1996.

[19] J. L. Thomason and L. J. Adzima, "Sizing up the interphase: an insider's guide to the science of sizing," *Compos. Part A: Appl Sci Manuf*, vol. 32, no. 3-4, pp. 313–321, 2001.

[20] B. Fibreglass", "Sizing application." Obtained from James L. Thomason with permission from 3B, 2014.

[21] F. R. Jones, "A review of interphase formation and design in fibre-reinforced composites," *J. Adhes. Sci. Technol.*, vol. 24, no. 1, pp. 171–202, 2010.

[22] M. Tanoglu, S. Ziaee, S. H. McKnight, G. R. Palmese, and J. W. Gillespie, "Investigation of properties of fiber / matrix interphase formed due to the glass fiber sizings," *J. Mater. Sci.*, vol. 36, no. 12, pp. 3041–3053, 2001.

[23] S. Feih, J. Wei, P. Kingshott, and B. F. Sørensen, "The influence of fibre sizing on the strength and fracture toughness of glass fibre composites," *Compos. Part A: Appl Sci Manuf*, vol. 36, no. 2, pp. 245–255, 2005.

[24] X. Liu, J. L. Thomason, and F. R. Jones, "Xps and afm study of interaction of organosilane and sizing with e-glass fibre surface," *J. Adhes.*, vol. 84, no. 4, pp. 322–338, 2008.

[25] R.-C. Zhuang, T. Burghardt, and E. Mäder, "Study on interfacial adhesion strength of single glass fibre/polypropylene model composites by altering the nature of the surface of sized glass fibres," *Compos. Sci. Technol.*, vol. 70, no. 10, pp. 1523–1529, 2010.

[26] S. Mallerino, J. F. Chailan, and L. J. Vernet, "Glass fibre sizing effect on dynamic mechanical properties of cyanate ester composites i. single frequency investigations," *Eur. Polym. J.*, vol. 41, no. 8, pp. 1804–1811, 2005.

[27] H. F. Wu, D. W. Dwight, and N. T. Huff, "Effects of silane coupling agents on the interphase and performance of glass-fiber-reinforced polymer composites," *Compos. Sci. and Technol.*, vol. 57, no. 8, pp. 975–983, 1997.

[28] M. Öhman and D. Persson, "Atr-ftir kretschmann spectroscopy for interfacial studies of a hidden aluminum surface coated with a silane film and epoxy i. characterization by irras and atr-ftir," *Surf. Interface Anal.*, vol. 44, no. 2, pp. 133–143, 2011.

[29] S. Rudzinski, L. Häussler, C. Harnisch, E. Mäder, and G. Heinrich, "Glass fibre reinforced polyamide composites: Thermal behaviour of sizings," *Compos. Part A: Appl Sci Manuf*, vol. 42, no. 2, pp. 157–164, 2011.

[30] L. Salmon, F. Thorminette, M. F. Pays, and J. Verdu, "Hydrolytic degradation of model networks simulating the interfacial layers in silane-coupled epoxy/glass composites," *Compos. Sci. and Technol.*, vol. 57, no. 8, pp. 5245–5252, 1997.

[31] M. G. González, J. C. Cabanelas, and J. Baselga, "Applications of ftir on epoxy resins – identification, monitoring the curing process, phase separation and water uptake," in *Infrared Spectroscopy - Materials Science, Engineering and Technology* (T. Theophanides, ed.), ch. 13, pp. 261–284, Rijeka, Croatia: InTech, 2012.

[32] G. Xue, S. Lie, and S. Jiang, "The studies of the curing of an epoxy resin on copper wire by ftir external reflection spectroscopy," *Chinese J. Polym. Sci.*, vol. 6, no. 51-55, pp. 505–538, 1988.

[33] F. Fouchal, J. A. G. Knight, and P. M. Dickens, "Monitoring the polymerization of a diglycidyl ether bisphenol-a/2,2'-dimethyl-4,4'-methylenebis (cyclohexylamine) matrix with a fourier transform infrared optical fibre sensor," in *Proceedings of the Institution of Mechanical Engineers, Part L: Journal of Materials: Design and Applications*, pp. 331–342, 2005.

[34] A. Dupont, "Characterization of silicones," in *Inorganic polymers* (R. De Jaeger and M. Gleria, eds.), Hauppauge, United States of America: Nova Science Publishers, 2007.

[35] L. T. Zhuravlev, "The surface chemistry of amorphous silica. zhuravlev model," *Colloids Surf. A: Physicochem Eng. Asp.*, vol. 173, no. 1-3, pp. 1–38, 2000.

[36] J. Macan, H. Ivanković, M. Ivanković, and H. J. Mencer, "Study of cure kinetics of epoxy-silica organic–inorganic hybrid materials," *Thermochim. Acta*, vol. 414, no. 2, pp. 219–225, 2004.

[37] Y. Kusano, H. Mortensen, B. Stenum, P. Kingshott, T. L. Andersen, J. Brøndsted, P. Bilde-Sørensen, B. Sørensen, and H. Bindslev, "Atmospheric pressure plasma treatment of glass fibre composite for adhesion improvement," *Plasma Process. Polym.*, vol. 4, pp. 455–459, 2007.

[38] L. Yang and J. L. Thomason, "Development and application of micromechanical techniques for characterising interfacial shear strength in fibre-thermoplastic composites," *Polymer Testing*, vol. 31, no. 7, pp. 895–903, 2012.

[39] M. R. Piggott, "Failure processes in the fibre-polymer interphase," *Composites Science and Technology*, vol. 42, no. 1-3, pp. 57–76, 1991.

[40] J. L. Thomason and L. Yang, "Temperature dependence of the interfacial shear strength in glass-fibre epoxy composites," *Compos. Sci. and Tech.*, vol. 96, pp. 7–12, 2014.

[41] L. Yang and J. L. Thomason, "Interface strength in glass fibre-polypropylene measured using the fibre pull-out and microbond methods," *Compos. Part A: Appl Sci Manuf*, vol. 41, no. 9, pp. 1077–1083, 2010.

[42] J. L. Thomason and L. Yang, "Temperature dependence of the interfacial shear strength in glass fibre polypropylene composites," *Compos. Sci. and Tech.*, vol. 71, no. 13, pp. 1600–1605, 2011.

[43] A. Strong, "Chapter 4: Epoxies," in *Fundamentals of Composites Manufacturing – Materials, Methods and Application* (A. Strong, ed.), pp. 85–112, Michigan, USA: Society of Manufacturing Engineers, 2007.

[44] A. Pegoretti, C. Della Volpe, M. Detassis, C. Migliaresi, and H. D. Wagner, "Thermomechanical behaviour of interfacial region in carbon fibre/epoxy composites," *Compos. Part A: Appl Sci Manuf*, vol. 27, no. 11, pp. 1067–1074, 1996.

[45] L. DiLandro and M. Pegoraro, "Evaluation of residual stresses and adhesion in polymer composites," *Compos. Part A: Appl Sci Manuf*, vol. 27, no. 9, pp. 847–853, 1996.

[46] J. L. Thomason, L. Yang, D. Bryce, and R. Minty, "An exploration of the relationship of chemical and physical parameters in the micromechanical characterisation of the apparent interfacial strength in glass fibre epoxy systems," *IOP Conf. Series: Mat. Sci. Eng.*, vol. 139, no. 1, p. 012048, 2016.

[47] J. Jakobsen, M. Jensen, and J. H. Andreasen, "Thermo-mechanical characterisation of in-plane properties for csm e-glass epoxy polymer composite materials - part 1: Thermal and chemical strain," *Polymer Testing*, vol. 32, no. 8, pp. 1350–1357, 2013.

[48] L. Khoun and P. Hubert, "Cure shrinkage characterization of an epoxy resin system by two in situ measurement methods," *Polym. Compos.*, vol. 31, no. 9, pp. 1603–1610, 2010.

[49] J.-P. Pascault and R. Williams, eds., *Epoxy Polymers – New Materials and Innovations*. Weinheim, Germany: Wiley-VCH, 2010.

[50] F. G. Garcia, B. G. Soares, V. Pita, R. Sánchez, and J. Rieumont, "Mechanical properties of epoxy networks based on dgeba and aliphatic amines," *J. Appl. Polym. Sci.*, vol. 106, no. 3, pp. 2047–2055, 2007.

[51] M. Nishikawa, T. Okabe, K. Hemmi, and N. Takeda, "Micromechanical modeling of the microbond test to quantify the interfacial properties of fiber-reinforced composites," *International Journal of Solids and Structures*, vol. 45, no. 14-15, p. 4098–4113, 2008.

[52] E. P. Plueddemann, "Principles of interfacial coupling in fibre-reinforced plastics," *Int. J. Adhes. Adhes.*, vol. 1, no. 6, pp. 305–310, 1981.

[53] S. Shokoohi, A. Arefazar, and R. Khosrokhavar, "Silane coupling agents in polymer-based reinforced composites: A review," *J. Reinf. Plast. Compos.*, vol. 27, no. 5, pp. 473–485, 2008.

[54] D. J. Montgomery and W. T. Milloway, "The vibroscopic method for determination of fiber cross-sectional area," *Textile Research Journal*, vol. 22, no. 11, pp. 729–735, 1952.

[55] D. M. Laura, H. Keskkula, J. W. Barlow, and D. R. Paul, "Effect of glass fiber surface chemistry on the mechanical properties of glass fiber reinforced , rubber-toughened nylon 6," *Polymer*, vol. 43, pp. 4673–4687, 2002.

[56] A. Valadez-Gonzalez, J. Cervantes-Uc, R. Olayo, and P. Herrera-Franco, "Effect of fiber surface treatment on the fiber–matrix bond strength of natural fiber reinforced composites," *Composites Part B: Engineering*, vol. 30, no. 3, pp. 309–320, 1999.

[57] P. Herrera-Franco and A. Valadez-González, "A study of the mechanical properties of short natural-fiber reinforced composites," *Composites Part B: Engineering*, vol. 36, no. 8, pp. 597–608, 2005.

[58] M. Abdelmouleh, S. Boufi, M. Belgacem, and A. Dufresne, "Short natural-fibre reinforced polyethylene and natural rubber composites: Effect of silane coupling agents and fibres loading," *Composites Science and Technology*, vol. 67, no. 7-8, pp. 1627–1639, 2007.

[59] A. Vazquez, M. Ambrustolo, S. M. Moschiar, M. M. Reboredo, and J. F. Gcrardb, "Interphase modification in unidirectional glass-fibre epoxy composites," *Composites Science and Technology*, vol. 58, pp. 549–558, 1998.

[60] D. Wang, F. Jones, and P. Denison, "A TOF-SIMS study of the incorporation of aluminium into the silane coating on E-glass fibres," *Catalysis Today*, vol. 12, pp. 375–383, 1992.

[61] C. A. Angell, "Thermal degradation and evolved gas analysis: A polymeric blend of urea formaldehyde (uf) and epoxy (dgeba) resin," *Arabian Journal of Chemistry*, vol. 7, no. 6, pp. 1140–1147, 2014.

[62] W. H. Otto, "Compaction effects in glass fibers," *Journal of The American Ceramic Society*, vol. 44, no. 2, pp. 68–72, 1961.

[63] L. Yang and J. L. Thomason, "Effect of silane coupling agent on mechanical performance of glass fibre," *Journal of Materials Science*, vol. 48, no. 5, pp. 1947–54, 2012.

[64] W. Brearley and D. G. Holloway, "The effect of heat-treatment on breaking strength of glass," *Physics and Chemistry of Glasses*, vol. 4, no. 3, pp. 69–75, 1963.

[65] S. Feih, E. Boiocchi, G. Mathys, Z. Mathys, A. G. Gibson, and A. P. Mouritz, "Mechanical properties of thermally-treated and recycled glass fibres," *Composites Part B*, vol. 42, no. 3, pp. 350–8, 2011.

[66] P. G. Jenkins, L. Yang, J. J. Liggat, and J. L. Thomason, "Investigation of the strength loss of glass fibre after thermal conditioning," *J Mater Sci*, vol. 50, pp. 1050–7, 2015.

[67] P. Zinck, M. F. Pays, R. Rezakhanlou, and J. F. Gerard, "Mechanical characterisation of glass fibres as an indirect analysis of the effect of surface treatment," *J. Mater. Sci.*, vol. 34, no. 9, pp. 2121–2133, 1999.

[68] P. Zinck, E. Mäder, and J. F. Gerard, "Role of silane coupling agent and polymeric film former for tailoring glass fiber sizings from tensile strength measurements," *J. Mater. Sci.*, vol. 36, no. 21, pp. 5245–5252, 2001.

[69] E. Mäder, S.-L. Gao, and R. Plonka, "Static and dynamic properties of single and multi-fiber/epoxy composites modified by sizings," *Composites Science and Technology*, vol. 67, no. 6, pp. 1105–1115, 2007.

[70] T. L. Anderson, *Fracture mechanics: fundamentals and applications*. Boca Raton, Florida, United States: CRC Press, 2005.

[71] J. R. Rice, "A path independent integral and the approximate analysis of strain concentration by notches and cracks," *Journal of Applied Mechanics,*, vol. 35, no. 2, pp. 379–386, 1968.

[72] H. Yoshihara, "Simple estimation of critical stress intensity factors of wood by tests with double cantilever beam and three-point end-notched flexure," *Holzforschung*, vol. 61, no. 2, p. 182–189, 2007.

[73] M. Tanaka, G. Firard, E. Davis, A. Peuto, and N. Bignell, "Recommended table for the density of water between 0 °c and 40 °c based on recent experimental reports," *Metrologia*, vol. 38, no. 4, p. 301, 2001.

[74] B. F. Sørensen, A. Horsewell, O. Jørgensen, A. N. Kumar, and P. Engbæk, "Fracture resistance measurement method for *in situ* observation of crack mechanisms," *J. Am. Ceram. Soc.*, vol. 81, no. 3, p. 661–69, 1998.

[75] X. Gao, J. W. Gillespie, R. E. Jensen, W. Li, B. Haque, and S. McKnight, "Effect of fiber surface texture on the mechanical properties of glass fiber reinforced epoxy composite," *Compos. Part A: Appl Sci Manuf*, vol. 74, pp. 10–17, 2015.

[76] M. Oldenbo, S. P. Fernberg, and L. A. Berglund, "Mechanical behaviour of smc composites with toughening and low density additives," *Compos. Part A: Appl Sci Manuf*, vol. 34, no. 9, pp. 875–885, 2003.

[77] B. F. Sørensen and T. K. Jacobsen, "Characterizing delamination of fibre composites by mixed mode cohesive laws," *Composites Science and Technology*, vol. 69, no. 3-4, pp. 445–456, 2009.

[78] M. Rask and B. F. Sørensen, "Determination of the j integral for laminated double cantilever beam specimens: The curvature approach," *Engineering Fracture Mechanics*, vol. 96, pp. 37–48, 2012.

Published by:
DTU Nanotech
Department of Micro- and Nanotechnology
Technical University of Denmark
Ørsteds Plads, building 345C
DK-2800 Kgs. Lyngby